Inorganic Chemistry

Article

Cite This: Inorg. Chem. 2017, 56, 13679-13696

pubs.acs.org/IC

Synthesis and Biological Evaluation of Ru(II) and Pt(II) Complexes Bearing Carboxyl Groups as Potential Anticancer Targeted Drugs

Mª Ángeles Martínez,[*,†,‡] M. Pilar Carranza,[⊥] Anna Massaguer,[*,‡] Lucia Santos,[#] Juan A. Organero,[○] Cristina Aliende,[∥] Rafael de Llorens,[‡] Iteng Ng-Choi,[§] Lidia Feliu,[§] Marta Planas,[§] Ana M. Rodríguez,[▽] Blanca R. Manzano,[⊥] Gustavo Espino,[*,∥] and Félix A. Jalón[*,⊥]

[†]Department of Chemistry, University of Girona, Campus Montilivi, 17003 Girona, Catalunya, Spain

[‡]Department of Biology, University of Girona, Campus Montilivi, 17003 Girona, Catalunya, Spain

[§]Laboratori d'Innovació en Processos i Productes de Síntesi Orgànica (LIPPSO), Department of Chemistry, University of Girona, Campus Montilivi, 17003 Girona, Catalunya, Spain

[∥]Universidad de Burgos. Dpto de Química, Facultad de Ciencias, Pza. Misael Bañuelos s/n, 09001 Burgos, Spain

[⊥]Universidad de Castilla-La Mancha, Facultad de Ciencias y Tecnologías Químicas-IRICA, Avda. Camilo J. Cela 10, 13071 Ciudad Real, Spain

[#]Universidad de Castilla-La Mancha, Departamento de Química Física, Avda. Camilo J. Cela s/n, 13071 Ciudad Real, Spain

[○]Universidad de Castilla-La Mancha, Departamento de Química Física, Facultad de Ciencias Ambientales y Bioquímica, and INAMOL, Avenida Carlos III, S.N., 45071 Toledo, Spain

[▽]Universidad de Castilla-La Mancha, Escuela Técnica Superior de Ingenieros Industriales, Avda. Camilo J. Cela, 13071 Ciudad Real, Spain

Supporting Information

ABSTRACT: The synthesis and characterization of Pt(II) (**1** and **2**) and Ru(II) arene (**3** and **4**) or polypyridine (**5** and **6**) complexes is described. With the aim of having a functional group to form bioconjugates, one uncoordinated carboxyl group has been introduced in all complexes. Some of the complexes were selected for their potential in photodynamic therapy (PDT). The molecular structures of complexes **2** and **5**, as well as that of the sodium salt of the 4′-(4-carboxyphenyl)-2,2′:6′,2″-terpyridine ligand (cptpy), were determined by X-ray diffraction. Different techniques were used to evaluate the binding capacity to model DNA molecules, and MTT cytotoxicity assays were performed against four cell lines. Compounds **3**, **4**, and **5** showed little tendency to bind to DNA and exhibited poor biological activity. Compound **2** behaves as bonded to DNA probably through a covalent interaction, although its cytotoxicity was very low. Compound **1** and possibly **6**, both of which contain a cptpy ligand, were able to intercalate with DNA, but toxicity was not observed for **6**. However, compound **1** was active in all cell lines tested. Clonogenic assays and apoptosis induction studies were also performed on the PC-3 line for **1**. The photodynamic behavior for complexes **1**, **5**, and **6** indicated that their nuclease activity was enhanced after irradiation at λ = 447 nm. The cell viability was significantly reduced only in the case of **5**. The different behavior in the absence or presence of light makes complex **5** a potential prodrug of interest in PDT. Molecular docking studies followed by molecular dynamics simulations for **1** and the counterpart without the carboxyl group confirmed the experimental data that pointed to an intercalation mechanism. The cytotoxicity of **1** and the potential of **5** in PDT make them good candidates for subsequent conjugation, through the carboxyl group, to "selected peptides" which could facilitate the selective vectorization of the complex toward receptors that are overexpressed in neoplastic cell lines.

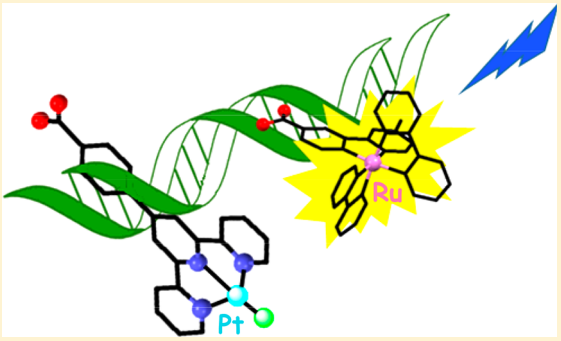

INTRODUCTION

In the past few decades, researchers have focused a great deal on finding new metal-based anticancer drugs to discover alternative chemotherapies to those based on cisplatin.[1] The main reasons for this search, with the aim of overcoming the limitations of cisplatin drugs,[2,3] are as follows: (i) to reduce toxicity further, (ii) to circumvent resistance, and (iii) to increase selectivity.

Two important approaches to increase selectivity are the use of photodynamic therapy (PDT)[4,5] and the formation of bioconjugates to control release and drug targeting.[6]

Photoactive agents are very attractive, since they allow spatial and temporal control of the antitumor activity of drugs. Ideally, in

Received: May 9, 2017
Published: November 3, 2017

DOI: 10.1021/acs.inorgchem.7b01178
Inorg. Chem. 2017, 56, 13679−13696

such cases, the compounds would act as prodrugs and cytotoxicity would occur only when the compounds are exposed to light. High specificity is achieved through PDT, and different types of cancer have been treated.[7,8] Transition-metal complexes containing polypyridyl ligands appear to be particularly attractive as photoreactive agents.[9−12]

The functionalization of drugs with reactive chemical groups that are suitable for the preparation of bioconjugates with active protein-vectors opens up the opportunity for the delivery of such substances to the most appropriate target.[13] These proteins are able to recognize specific receptors that are overexpressed on the surface of cancer cells[6] facilitating, in this way, the tumor-specific accumulation of the drug.[14,15]

Considering this concept, we decided to synthesize a set of complexes including the attachment of a carboxyl group in one ligand, on the basis that the presence of this binding group offered the possibility of increasing drug specificity toward cancer cells through conjugation to a carrier peptide. Additionally, some of the complexes were designed to have the possibility of being activated in the presence of light (PDT). Taking into account these ideas and the previous antitumoral activity of different Pt,[16,17] polypyridyl,[10,11] and arene Ru[17−21] compounds, the complexes chosen were those shown in Chart 1.

Chart 1. Complexes 1−6 and Atom Numbering of the Ligands

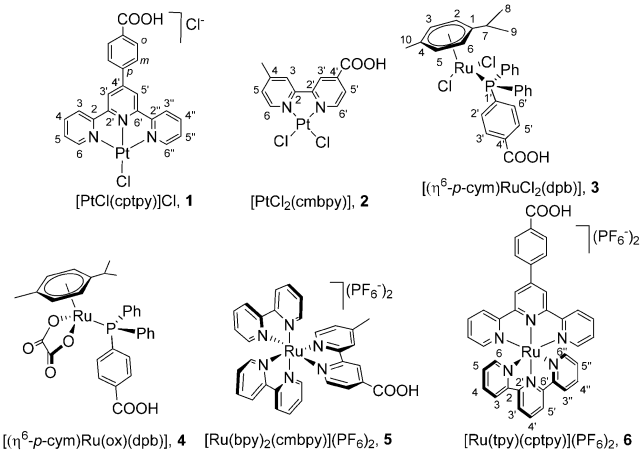

Prior to the formation of bioconjugates, which are candidates for future developments, and with the aim of obtaining a selection of the most promising candidates, the interaction of complexes **1**−**6** with DNA was studied in this work by a variety of techniques. The complexes were also tested against human tumor cell lines of different origins. Photoactivation of complexes **1**, **5**, and **6** and their influence on antiproliferative activity were also addressed. Computational studies such as molecular docking and MDS (molecular dynamics simulations) were carried out to obtain information about the binding modes to DNA.

RESULTS AND DISCUSSION

Synthesis of Ligands and Complexes. The ligands functionalized with carboxyl groups used for the preparation of complexes are shown in Scheme 1. Ligand dpb was purchased commercially, and this has previously been used as a terminal phosphorus donor in the preparation of asymmetric ligands.[22] Ligand cptpy was prepared by adapting different reported procedures for its synthesis.[23,24] Ligand cmbpy was prepared by an analogous procedure to that reported in the literature, with a significant improvement in the purification of the resulting solid.[25,26]

Complexes **1**−**6** were prepared by conventional synthetic methods, as depicted in Scheme 1. The cation complex of **1** was previously prepared as the PF_6 salt[27] in DMF under reflux with a moderate yield (49%). In this work, we prepared complex **1** as the Cl salt by a different and milder method that involved the reaction of cptpy with the $K_2[PtCl_4]$ salt in DMF (65 °C, 76% yield). Similarly, complex **2** was prepared by the reaction of cmbpy and $K_2[PtCl_4]$ in water. Complex **3** was easily prepared by the reaction of $[(\eta^6\text{-}p\text{-cymene})Ru(\mu\text{-Cl})Cl]_2$ with dpb in a 1:2 molar ratio in dichloromethane. Complex **4** was obtained in a one-pot reaction by treating a methanolic solution of the same dimeric precursor with $[Ag_2(C_2O_4)]$ followed, after filtration, by the addition of ligand dpb in a 1:2 molar ratio. Complexes **5**[28,29] and **6**[30] were previously prepared, but the methodology described herein for **6** is simpler and leads to a higher yield (86% versus 55%). Complex **6** was prepared by the reaction of $[RuCl_3(tpy)]$ with the ligand cptpy after the Ru complex had been activated at 60 °C with AgTfO in a EtOH/DMF mixture (see Scheme 1).

All of the complexes were isolated in moderate to good yields (from 50 to 90%) as yellow, orange, or brown solids that were air and moisture stable. With the exception of compound **3**, all products are insoluble or sparingly soluble in almost all organic solvents and in water. The solubility of the compounds in DMSO facilitates the preparation of $DMSO/H_2O$ solutions containing ≤5% of DMSO, and this makes biological studies of these complexes viable. Complex **3** is soluble in acetone, dichloromethane, and methanol, only partially soluble in ethanol, and insoluble in nonpolar organic solvents and water.

Characterization of Complexes. All of the complexes were characterized by ^1H, $^{13}C\{^1H\}$, $^{31}P\{^1H\}$ (**3** and **4**) NMR and IR spectroscopy, and **3** and **4** were also studied by FAB^+ mass spectrometry. The molecular and crystalline structure of the Na salt of ligand cptpy and those of complexes **2** and **5** were determined by X-ray diffraction.

The FAB^+ mass spectra of the neutral complexes **3** and **4** show the peak corresponding to the molecular mass plus a proton, together with peaks corresponding to the loss of the *p*-cymene and the anionic ligands.

The assignment of the NMR resonances was facilitated in some cases by bidimensional experiments such as gCOSY, NOESY, gHSQC, and gHMBC. The NMR data, with the corresponding assignments, are reflected in the experimental section. The assignment for complexes **1** and **6** is also included because in the literature the resonances are not assigned (**1**) or only partially assigned (**6**).

The ^1H and $^{13}C\{^1H\}$ NMR spectra of complexes **3** and **4** reveal a C_s local symmetry, with a characteristic AA′BB′ spin system for the aromatic protons of the *p*-cymene (*p*-cym) group and a doublet for the homotopic methyl hydrogens of the isopropyl group. As expected, the $^{31}P\{^1H\}$ NMR spectra of derivatives **3** and **4** exhibit a single singlet. This resonance appears at higher field in **3** than in **4**—as observed in other $RuCl_2$(arene) and Ru(oxalate)(arene) counterparts.[31,32] The resonances in the ^1H NMR spectrum of **2** were assigned on the basis of the COSY spectrum and some nOes observed (see red arrows in Scheme 1).

Hydrolysis Processes of 1−3. The possible hydrolysis of the chlorido complexes **1**−**3** was analyzed. A CD_3SOCD_3 solution of **1** kept unchanged for 1 day (Figure S1). The addition of D_2O, until a CD_3SOCD_3:D_2O ratio of 5:1, shifted the resonances to high field. In order to discard the existence of a fast equilibrium of **1** with aquo-species, a solution of NaCl in D_2O was added. A further shift of the resonances to high field was observed, supporting the fact that the chemical shift change is a solvent effect and not a

DOI: 10.1021/acs.inorgchem.7b01178
Inorg. Chem. 2017, 56, 13679−13696

Scheme 1. Synthesis of Complexes 1−6[a]

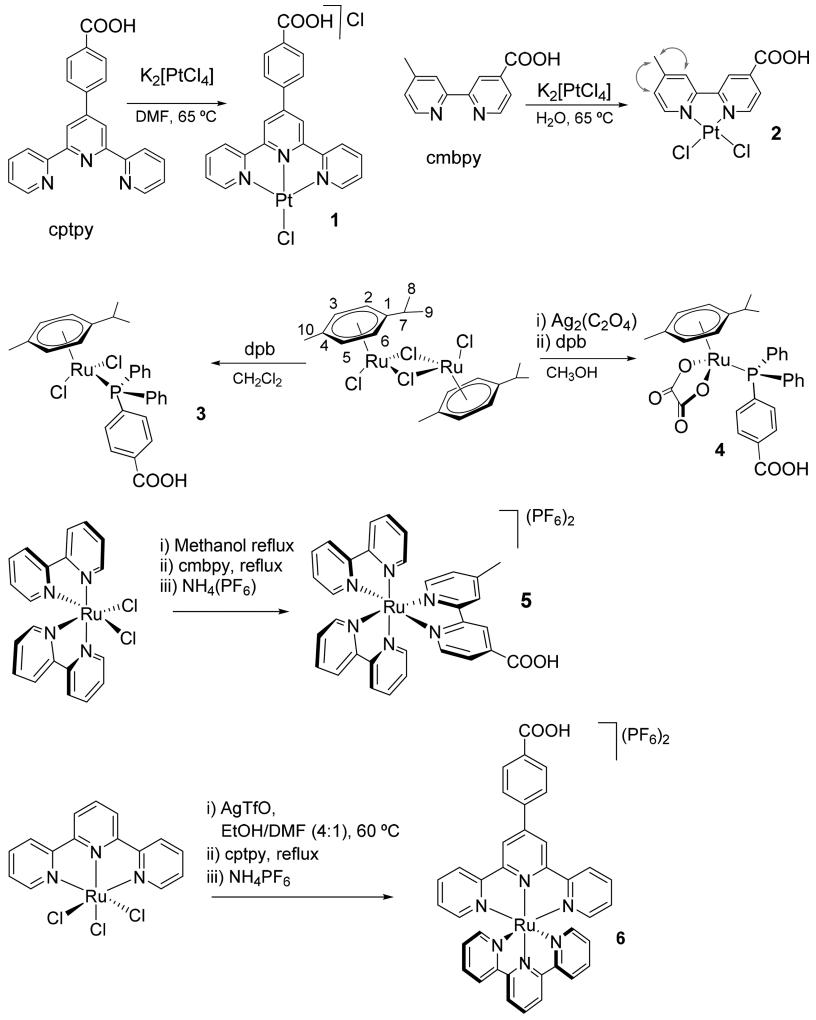

[a]The red arrows in **2** represent observed nOes.

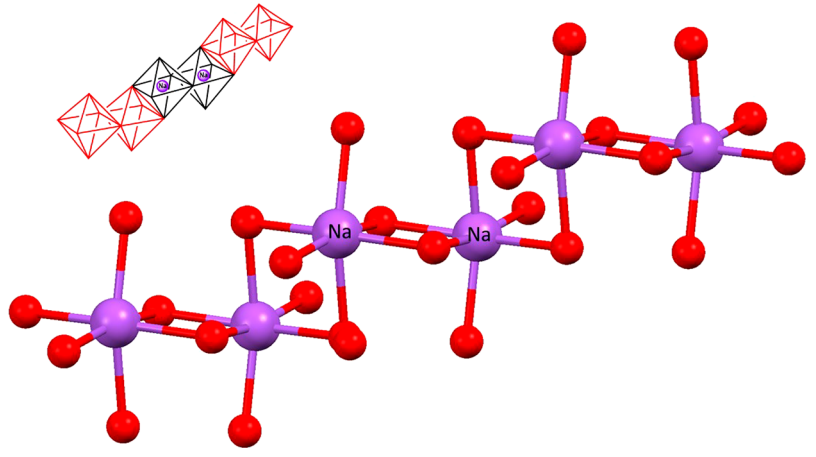

Figure 1. Molecular representation of the polymer $[Na(OH_2)_2(\mu^2\text{-}OH_2)_2]_n$ in the salt $[Na(H_2O)_4]$cptpy·H_2O. Hydrogen atoms have been omitted for clarity.

consequence of a rapid aquation−anation equilibrium. In the case of **2**, a CD_3SOCD_3 solution did not change after 3 days. However, the addition of increasing amounts of water (up to a CD_3SOCD_3:H_2O ratio of 5:1) led, besides to a shift to high field of the resonances of **2**, to the instantaneous and increasing formation of two new minor species in an equimolar ratio (final 70:15:15 ratio with **2** being the major species, see Figure S2). We propose that these compounds arise due to water exchange of one of the two different chloride ligands. A methanol solution of **3** did not evolve after 3 days. Once again, the addition of water (CD_3OD:H_2O ratio of 10:1) led to the instantaneous formation of two minor species in a 93:5:2 ratio (**3** is the major species). The number of new

DOI: 10.1021/acs.inorgchem.7b01178
Inorg. Chem. 2017, 56, 13679−13696

p-cymene signals indicated the formation of an asymmetric and a symmetric species (see Figure S3). We propose that in this case the consecutive hydrolysis of one or two chloride ligands had taken place. The new species have also been observed by $^{31}P\{^{1}H\}$NMR (Figure S4).

It is important to note that the carboxyl group could be deprotonated at the pH of the biological studies, a fact that will increase in one unit the negative charge of the complexes interfering the interaction with DNA. However, the observed easy hydrolysis of compounds **2** and **3** would lead to an increase of the positive charge.

Solid State Structure. The molecular and crystalline structures of the Na^+ salt of the ligand cptpy with five water molecules and those of the complexes **2**·2DMF and **5**·acetone were determined by X-ray diffraction. The main crystal data and structure refinement parameters are given in the Supporting Information.

[Na(H$_2$O)$_4$]cptpy·H$_2$O. The chemical structure is constituted by the polymeric species $[Na(OH_2)_2(\mu^2\text{-}OH_2)_2]_n^+$, a carboxylate ligand, and an additional water crystallization molecule. The cationic aqua–Na^+ polymeric complex, that constitutes a water channel with Na^+ cations along the crystallographic *b* axis, is formed by $[Na_2(OH_2)_6(\mu^2\text{-}OH_2)_2]$ dimers that auto assemble building a zigzag polymer (Figure 1). According to the CSD,[33,34] only two examples of this aqua–Na^+ polymeric structure have been reported previously. A complex framework of hydrogen bonds between adjacent water molecules of this polymer with the carboxylate units and with the water crystallization molecule of the cptpy seems to contribute to the stabilization of this water channel (Figure S5 and Table S1).

The cptpy cation is essentially flat (see the Supporting Information, Figure S6) with dihedral angles of 3.05 and 3.80° between central and lateral pyridine rings and of 8.12° between the former and the 4-benzoic acid ring. The C–C and C–N bond distances are in the range of those found in other tpy structures (see the Supporting Information).[35] The C–O distances are identical, 1.250(4) Å, and this indicates electronic delocalization.

***2*·2DMF.** The molecular structure of the neutral complex is depicted in Figures 2 and S7. In the unit cell, the asymmetric unit is formed by two independent molecules of the complex (A and B) together with four molecules of DMF. A and B have an essentially square planar geometry and are very similar, but there are some minor differences between them, for instance, in the NCCN torsion and bite angles. For the carboxyl groups, the two C–O bond distances, which are in the range 1.25–1.28 Å, are practically identical. Two molecules of type A and two of type B are aggregated in pairs by supramolecular contacts but in different arrangements (see Figures S8 and S9). These two arrangements are reminiscent of the two polymorphs of the $[PtCl_2(bpy)]$ complex, where the yellow variety exhibits isolated molecules with longer Pt–Pt distances (4.44 Å)[36] than the red polymorph, where linear chain aggregates are formed, and have shorter Pt–Pt distances (3.45 Å).[36,37] On the other hand, a third way of aggregating square planar polypyridine–Pt molecules as isolated pairs has been described, where the value of the Pt–Pt distance is intermediate. This is the case of the $[Pt(phen)_2]Cl_2\cdot 3H_2O$ with a Pt–Pt distance of 3.71 Å.[38] In the case of our complex, two different rearrangements appear in the same crystal with long Pt–Pt distances in the A pairs (4.84 Å) and short distances in the B pairs (3.64 Å). To the best of our knowledge, the existence of two different arrangements in the same crystal makes **2**·2DMF a unique example in the polymorphism of the polypyridine Pt derivatives. On the other hand, both A and B show hydrogen bonds with the crystallization DMF molecules, although in B the long distances suggest weaker interactions. The HCO group of DMF and the carboxyl groups in **2** are involved in these contacts (Figures S8 and S9).

***5*·acetone.** The asymmetric unit consists of a molecule of the dicationic complex, the corresponding two PF_6^- counteranions, and an acetone molecule of crystallization. Although complex **5** has been described previously,[28,29] its crystal structure has never been published before. In this structure, which is depicted in Figure 3, the ruthenium atom has a distorted octahedral geometry with angles between atoms in a *trans* disposition, N–Ru–N, in the range 172.02–174.51°. The two rings of the bpy or cmbpy ligands are practically in the same plane, with bite angles of 78.25 and 78.84° (bpy) or 80.56° (cmbpy). All of the Ru–N distances are in the range 2.034–2.061 Å. The carboxyl group of the cationic complex is involved in hydrogen bonds with

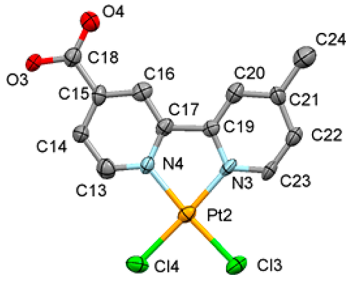

Figure 2. ORTEP diagram of one of the two independent molecules of complex **2** (type A in the text) at the 50% probability level. Selected bond distances (Å): Pt1–Cl1, 2.292(3); Pt1–Cl2, 2.295(3); Pt1–N1, 2.019(8); Pt1–N2, 2.060(7); C6–O1, 1.25(1); C6–O2, 1.27(1). Selected bond angles (deg): N1Pt1N2, 79.4(3); Cl1Pt1Cl2, 88.6(1); Cl1Pt1N2, 96.1(2); Cl2Pt1N1, 95.9(2); Cl1Pt1N1, 175.2(2); Cl2Pt1N2, 175.3(2). Hydrogen atoms have been omitted for clarity.

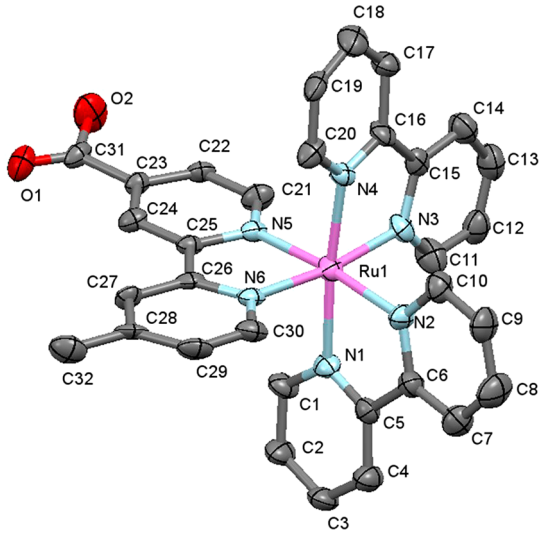

Figure 3. ORTEP diagram of the molecular cation complex **5** at the 50% probability level. Selected bond distances (Å): Ru1–N5, 2.020(8); Ru1–N6, 2.047(8); Ru1–N4, 2.059(9); Ru1–N3, 2.054(8); Ru1–N2, 2.058(9); Ru1–N1, 2.089(9). Bite angles (deg): N1–Ru1–N2, 78.0(4); N3–Ru1–N4, 78.3(4); N5–Ru1–N6, 80.6(4); C31–O1, 1.21(1); C31–O2, 1.37(1). Dihedral inter-py angles (deg): N1N2, 9.26, N3N4, 5.91, N5N6, 2.50. Hydrogen atoms have been omitted for clarity.

DOI: 10.1021/acs.inorgchem.7b01178
Inorg. Chem. 2017, 56, 13679–13696

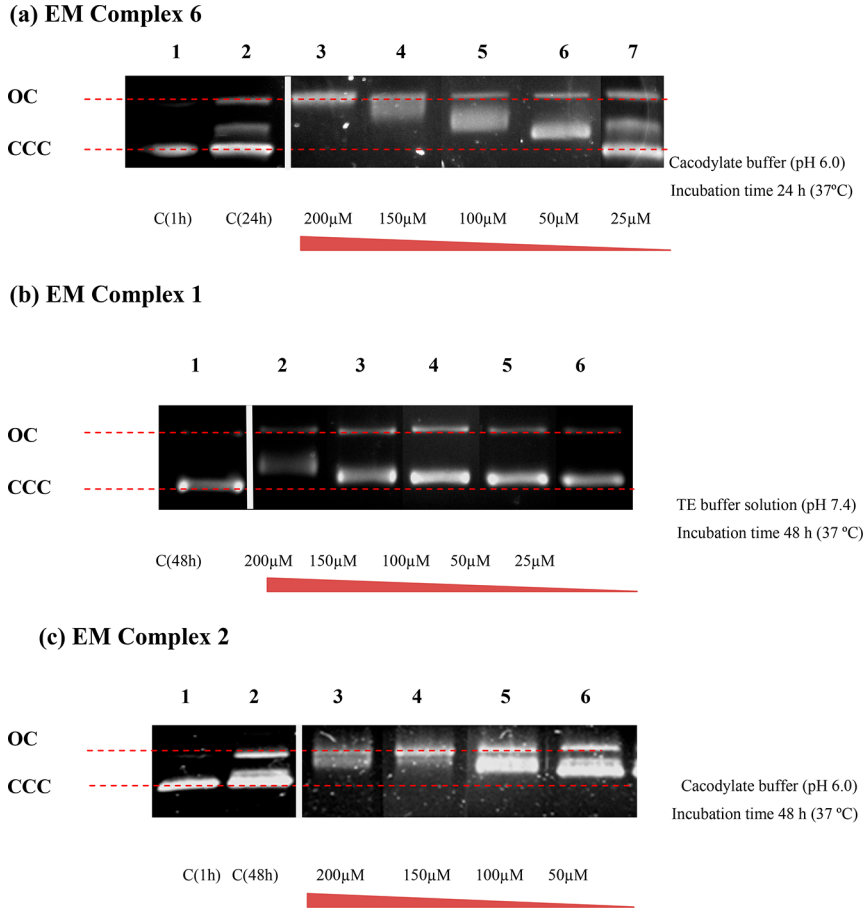

Figure 4. Agarose gel electrophoresis of supercoiled pUC18 plasmid DNA incubated in the presence of compound **1**, **2**, or **6** at the indicated concentrations. [pUC18 DNA] = 18.9 μM; C = pUC18 DNA incubated alone. Incubation time in parentheses. OC, relaxed open forms; CCC, covalently closed circular forms.

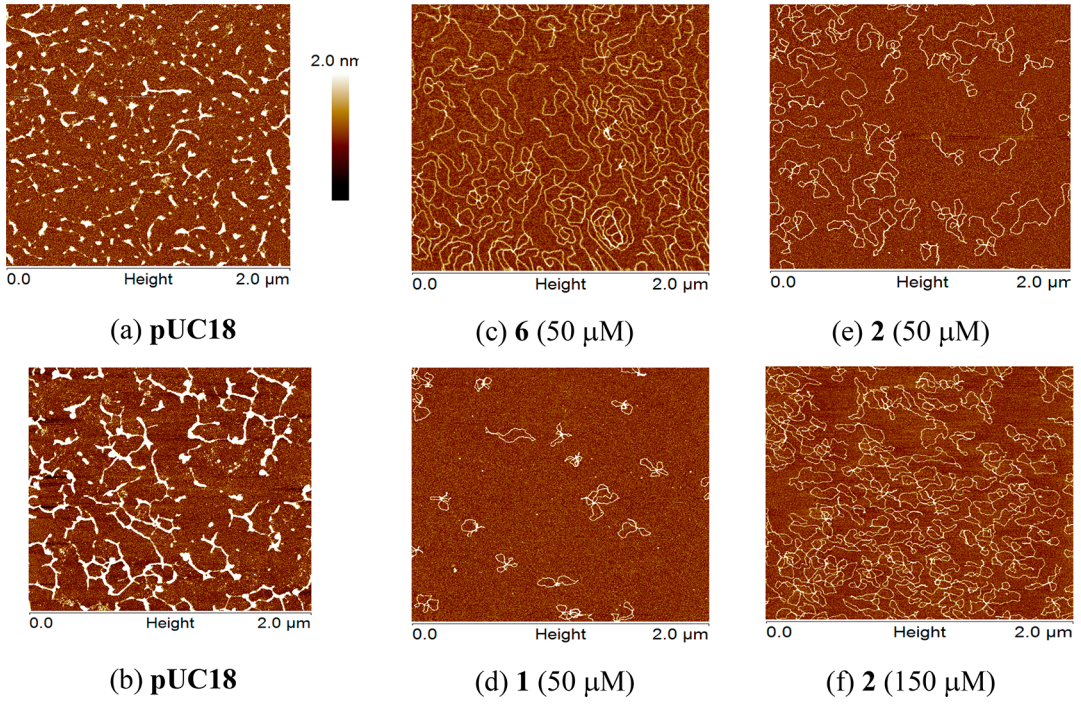

Figure 5. AFM analysis of the interaction of complexes **1**, **2**, and **6** with DNA in HEPES buffer solution (pH 7.4). Images of pUC18 plasmid alone (a, b) or incubated with **6** (50 μM, 24 h at 37 °C) (c); **1** (50 μM, 48 h at 37 °C) (d); or **2** (50 μM, 48 h at 37 °C) (e) and (150 μM) (f).

DOI: 10.1021/acs.inorgchem.7b01178
Inorg. Chem. 2017, 56, 13679−13696

the acetone molecule of crystallization with two interactions of different strength (see Figure S10).

DNA Interaction. The complexity of the DNA double helical structure offers various binding possibilities for a metal complex:[39] (i) by a covalent bond; (ii) by intercalation between adjacent base pairs; (iii) by interaction in the major or minor groove of the double helix. The electrostatic attraction of metal complexes with cationic charges aids binding to DNA in any case.

The mode and propensity of binding of the complexes to DNA (the main biological target) were studied in this work with the aid of agarose gel electrophoresis (to appreciate changes in the DNA tertiary structure) and atomic force microscopy (to visualize changes in the DNA topography and morphology). In both cases, the supercoiled pUC18 plasmid DNA was used. Furthermore, since compound **1** was the most promising of all the compounds in the cytotoxicity studies (see below), we also report fluorescence spectroscopy, viscosity measurements, and circular dichroism studies on this complex, which were carried out in order to understand better the DNA-binding mechanism.

Electrophoretic Mobility (EM) and Atomic Force Microscopy (AFM). EM experiments and direct visualization of the conformers of plasmid DNA using tapping mode atomic force microscopy (TMAFM) allow graphic evaluations of the plasmid DNA modifications caused by the interaction with metal complexes.[40,41]

Ruthenium polypyridyl complexes are generally described as particularly attractive DNA binders through electrostatic interactions, surface binding, or partial intercalation,[42] and Ru(arene) complexes through a covalent bond.[43] However, compounds **3**−**5** did not alter the electrophoretic mobility of plasmid DNA and this indicates the absence of an interaction with DNA (see Figure S11a−c). As a consequence, compounds **3**−**5** were not studied by AFM.

The results from EM and AFM experiments, under comparable conditions, for complexes **1**, **2**, and **6** are presented in Figures 4 and 5, respectively. The control experiments, i.e., in the absence of complexes, are also included in the first lanes for EM and in images a and b for AFM.

As represented in Figure 4a, treatment with increasing concentrations of compound **6** over 24 h progressively uncoiled the covalently closed circular (CCC) forms of pUC18 plasmid DNA. It should be noted that, after 24 h incubation in cacodylate buffer (pH 6.0) at 37 °C, an additional less compacted form of the pUC18 plasmid was also generated in the untreated control samples (see lane 2, Figure 4a and c). Interestingly, at the maximum concentration assayed (200 μM), complex **6** was able to induce total conversion of the DNA to its relaxed open (OC) form (lane 3). Similarly, in the corresponding AFM experiment carried out under the same conditions, complex **6** at a 50 μM concentration had already induced uncoiling of the CCC forms (Figure 5c). The relaxed DNA molecules distributed over the mica surface exhibited some structures with crossing points and/or knots, and some other structures with double strand scission. These effects could suggest a partial intercalating mode of DNA interaction.[44,45] In fact, compound **6** is an octahedral complex bearing the π-electronically extended and flat cptpy ligand, which is capable of stacking and partial intercalation in between base pairs. This fact, together with the overall charge, could provide the basis for interactions with DNA once the complex is appropriately oriented.

Higher incubation times (48 h) were required to observe a substantial effect of compounds **1** and **2** on the tertiary structure of the plasmid. Complex **1** induced minor changes in the electrophoretic pattern of the plasmid, and these were most evident when Tris−EDTA (TE) buffer solution (pH 7.4) was used as a buffer (Figure 4b), thus suggesting that the interaction barely affected the mobility and CCC/OC ratio of the plasmid DNA. Only at high concentrations (200 μM) did **1** generate a more relaxed slow-moving form of the plasmid (lane 2). The pK_a value of **1** described in the literature was 6.8−6.9,[46] and this reveals that the complex is essentially deprotonated at the experimental pH when Tris−EDTA (TE) was used (pH 7.4). Therefore, when cacodylate buffer (pH 6.0) is used, **1** should contain a protonated carboxylate, which could modify the mode of interaction with the DNA and explain the differences observed at these two pH values in the EM experiments. In AFM, more substantial effects were observed on the plasmid. Even at a concentration of 50 μM, under the same conditions as in the EM experiment, isolated DNA forms were generated with intramolecular loops (Figure 5d). These features are similar to those produced by intercalation agents based on planar heterocyclic ligands.[47]

A more evident interaction between **2** and DNA is shown in Figure 4c. Although the electrophoretic pattern of the plasmid is already modified at 50 μM (lane 6), treatment with increasing concentrations of this compound progressively transformed the supercoiled DNA to more relaxed forms (lanes 5−3). These results can be explained by the fact that complex **2** is potentially capable of promoting significant interactions with DNA through covalent bonds and thus high concentrations of the complex could lead to DNA aggregation due to cross-links. Image e in Figure 5 (**2**, 50 μM, 48 h at 37 °C) reveals that most of the DNA molecules are in an intermediate degree of folding. Besides, some molecules are in the OC form and some others appear with clear evidence of double strand scission. It can also be observed that some of the DNA structures are distorted due to the development of kinks, while others are cross-linked by **2**. This suggests that the effects of complex **2** are similar to those induced by cisplatin and its analogues,[2,10,48,49] which induce conformational changes in the plasmid DNA structure by covalent interactions between the metal and DNA. This may explain the greater DNA interaction of **2** according to Figure 4c. It can be seen from Figure 5f how intermolecular DNA aggregates become larger with increasing concentration of **2** (150 μM, 48 h at 37 °C), and the DNA molecules become more tightly packed, in accordance with the hypothesis introduced in the electrophoresis experiment.

Fluorescence Emission Spectroscopy. The binding of **1** was investigated by evaluating the fluorescence emission intensity of the ethidium bromide−DNA (EB−DNA) system upon addition of the compound.[35,50,51] As displayed in Figure S12, the addition of increasing concentrations of **1** to DNA previously treated with EB caused an appreciable reduction in the emission intensity of ca. 47%, which indicates that **1** binds to DNA in an intercalative way. The extent of the decrease in the emission intensity gives a measure of the binding affinity of **1** to DNA. The fluorescence quenching of EB bound to DNA by **1** yields a linear Stern−Volmer plot,[52] and this shows that **1** binds to DNA (Figure S13). The K_{app}[53] value for **1** is 1.06×10^6 M^{-1}, and this is high and comparable to other classical intercalator agents like acridine ($K_{app} = 1.5 \times 10^6$)[54] or actinomycin D ($K_{app} = 9.69 \times 10^5$).[55]

Viscosimetry Studies. In order to obtain further information on the binding of **1** to DNA, we carried out viscosity measurements on CT-DNA.[53,56,57]

DOI: 10.1021/acs.inorgchem.7b01178
Inorg. Chem. 2017, 56, 13679−13696

Table 1. Cytotoxicity of Complexes 1−6 against Cancer Cell Lines

	IC_{50}[a] (μM)						
	compound						
cell line	cisplatin	1	2	3	4	5	6
PC-3	2.5 ± 0.7	5.7 ± 1.6	>50	>50	>50	>50	>50
MCF-7	2.4 ± 0.4	27.3 ± 2.5	>50	>50	>50	>50	>50
CACO-2	8.9 ± 0.8	43.5 ± 3.5	>50	>50	n.d.	>50	>50
CAPAN-1	2.2 ± 0.3	38.4 ± 7.8	>50	46.3 ± 7.3	>50	>50	>50

[a]The IC_{50} values were determined by the MTT assay after 48 h of exposure to the compound. Data represent the mean ± SD of at least three independent experiments carried out in triplicate. n.d.: not determined.

The changes in the specific relative viscosity of DNA on addition of increasing concentrations of compound **1** are shown in Figure S14. The linear increase in viscosity of DNA produced by **1** suggests that the interaction of this compound involves classical intercalation.

Circular Dichroism (CD) Spectroscopy. Further support for the intercalative interaction of complex **1** with DNA was obtained by evaluating its behavior on CT-DNA by CD. CT-DNA shows a spectrum that is typical of the right-handed B-form, and it contains two bands: a positive band (275 nm) due to the base stacking and a negative band (245 nm) due to the right-handed helicity.[58] It is generally accepted that the classical intercalation enhances the base stacking and stabilizes helicity, thus increasing the intensities of both bands, whereas simple groove binding and electrostatic interaction of small molecules show lower, if any, perturbation on the base stacking and helicity bands.[59,60]

The CD spectra of CT-DNA, both alone and when incubated with complex **1** at 37 °C for 24 h at several molar ratios (r_i = 0.1, 0.3, 0.5), were recorded (Figure S15). A modest increase in the intensity of the positive band and a red shift of their maxima, with increasing values of r_i, were observed. For the negative band, an increase in the intensity of the band for r_i = 0.1 was observed, whereas a decrease was observed for r_i = 0.3 and 0.5. A blue shift in this band was observed.

The increase in the intensity of the stacking band could suggest the intercalation mode of binding, but the magnitude of the changes induced by **1** is not as significant as those described in the literature for other complexes binding to DNA in a classical intercalation mode.[60,61] The red shift in the λ_{max} has also been attributed to the action of intercalating agents.[58]

On the other hand, the decrease in the intensity of the DNA helicity band from r_i = 0.3 could indicate that complex **1** is involved in a hydrophobic interaction with the DNA surface, which in turn would promote certain conformational changes in DNA helicity.[62,63]

Taking into account the planar structure of **1** and the results obtained by AFM, EM, fluorescence emission spectroscopy, viscometry studies (see above), and CD, the intercalation of **1** between base pairs is the most reasonable option for the interaction between **1** and CT-DNA.

Biological Studies. *Cytotoxic Activity.* The antiproliferative activity of complexes **1−6** was tested against different human tumor cell lines: breast cancer (MCF-7), pancreatic cancer (CAPAN-1), prostate cancer (PC-3), and colon adenocarcinoma (CACO-2). Compounds were tested at different concentrations ranging from 0 to 100 μM to determine the concentration required to inhibit cell growth by 50% (IC_{50}). Compounds with IC_{50} values greater than 50 μM were considered to be inactive. Cisplatin was included as a control. It can be seen from the results in Table 1 that only complex **1** demonstrated an antiproliferative effect in all of the cancer cell lines analyzed, with IC_{50} values ranging from 5.7 to 43.5 μM. The best IC_{50} value was obtained in PC3 prostate cancer cells, and this result was similar to that of cisplatin in this cell line. Complexes **2** and **6** did not display any cytotoxic activity despite their ability to interact with DNA. It appears reasonable to propose that the lack of activity for these complexes could be related to their inability to cross the apolar cell membrane. Complexes **3**, **4**, and **5** did not show any interaction with DNA, and they also failed to induce cell cytotoxicity.

The long-term cytotoxic activity of compound **1** was also determined by measuring its ability to inhibit the clonogenic potential of cancer cells (Figure 6). Thus, PC-3 cells were treated for 6 or 24 h with complex **1** (5.5 μM) or cisplatin (2.5 μM) as a positive control, followed by plating at low density. Analysis of colony numbers after 10 days revealed that the inhibitory effect of **1** requires longer exposure times than cisplatin, since the number of colonies was only significantly reduced after 24 h of treatment

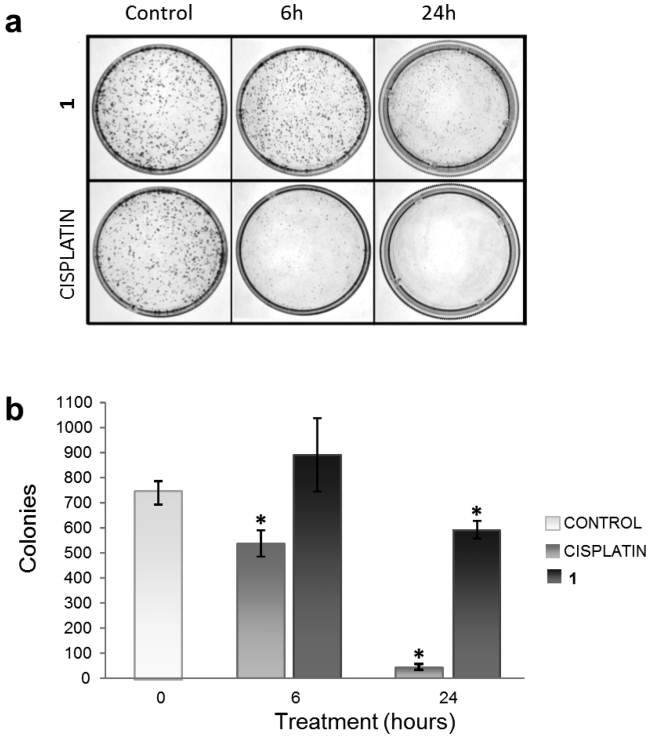

Figure 6. Clonogenic assay. (a) Colony formation of PC-3 cells after exposure to cisplatin and complex **1** (5.5 and 2.5 μM, respectively) for 6 or 24 h. (b) Bar charts showing the percentage of counted colonies relative to control untreated cells as the mean ± SD of three independent experiments. *p < 0.05 versus control cells.

DOI: 10.1021/acs.inorgchem.7b01178
Inorg. Chem. 2017, 56, 13679−13696

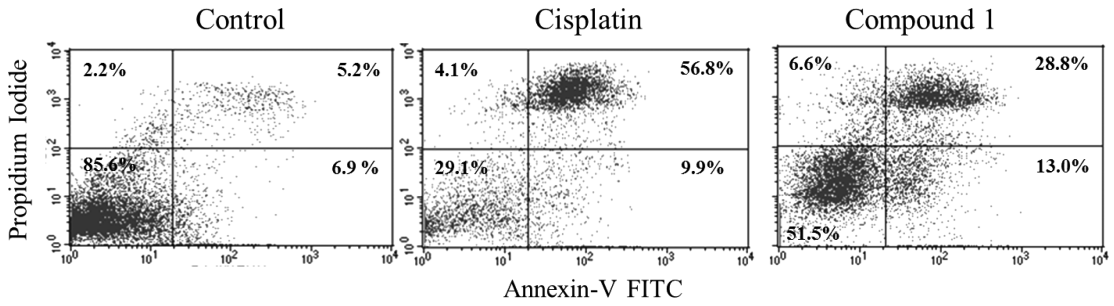

Figure 7. Apoptosis induction. PC-3 cells were treated with 25 μM **1** and cisplatin for 24 h, double stained with propidium iodide and Annexin V-FITC, and analyzed by flow cytometry. The *x*-axis shows Annexin V-FITC staining, and the *y*-axis indicates propidium iodide staining. The percentages of cells in each quadrant are indicated.

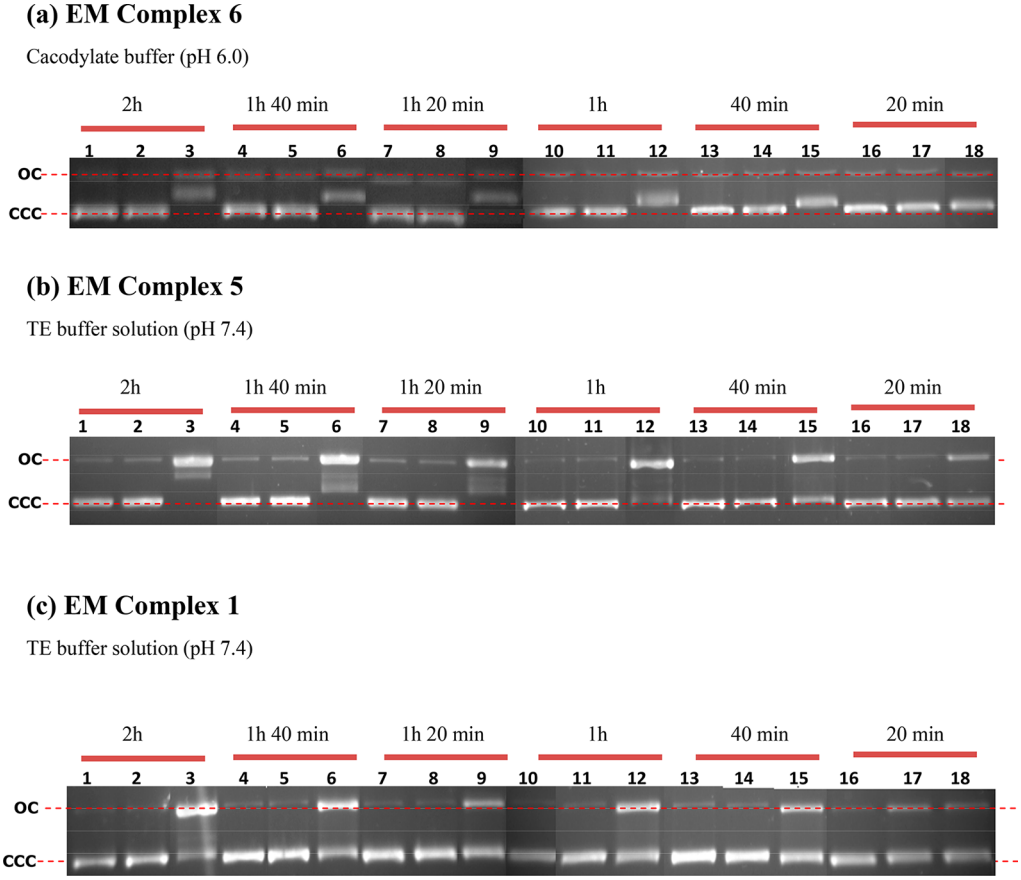

Figure 8. Agarose gel electrophoresis patterns of supercoiled pUC18 plasmid DNA ([pUC18DNA] = 18.9 μM) incubated in the presence of 50 μM complex **6** (a), **5** (b), or **1** (c), irradiated at λ = 447 nm at r.t. for different times. Lanes 1, 4, 7, 10, 13, and 16: DNA alone (light). Lanes 2, 5, 8, 11, 14, and 17: DNA + complex **6**, **5**, or **1** (dark). Lanes 3, 6, 9, 12, 15, and 18: DNA + complex **6**, **5**, or **1** (light). OC, relaxed open forms; CCC, covalently closed circular forms.

(by 23.7% compared with control cells). In contrast, exposure to cisplatin rapidly reduced the colony formation by 30.6% after 6 h of treatment and it was almost abolished after 24 h of treatment. These results reveal an inhibitory effect of **1** on the ability of cancer cells to proliferate and generate colonies. The activity of **1** is slower than that observed for cisplatin in this cell line, which indicates that the antitumoral effect takes place through a different mechanism. These observations are consistent with the previously described differences in the interaction of the compounds with the DNA.

Apoptosis Assays. To determine whether **1** induces cellular death through the activation of programed cell death (apoptosis) or necrosis, PC-3 cells were treated for 24 h with **1** and cisplatin at a concentration higher than the corresponding IC_{50} (25 μM) in order to force cell death induction. The cells were then analyzed by flow cytometry upon double annexin V/propidium iodide staining. As expected, most of the cells (56.8%) were in late apoptosis after cisplatin treatment. Similarly, compound **1** clearly induced apoptosis in PC-3 cells but with a slower cell death mechanism compared to cisplatin. As shown in Figure 7, after treatment with **1**, only 28.8% of cells were in late apoptosis, while 13.0% of the cells were still in early apoptosis. These findings are consistent with the slower cell death mechanism described in the clonogenic assays.

Photoactivation Assays and Effect on the Cytotoxic Activity. As stated in the Introduction, the use of visible light to

DOI: 10.1021/acs.inorgchem.7b01178
Inorg. Chem. 2017, 56, 13679−13696

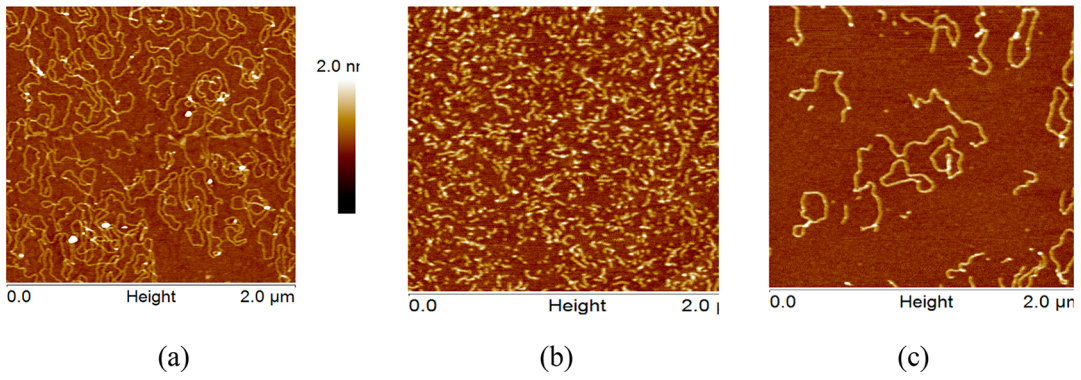

Figure 9. AFM images of pUC18 incubated in HEPES buffer solution (pH 7.4) at r.t. in the presence of 50 μM complex **6** (a), **5** (b), or **1** (c), irradiated at λ = 447 nm for 4 h.

activate a molecule and yield a potent drug is the base of photodynamic therapy.[64]

Complexes **1**, **5**, and **6** were selected due to the photophysical and photochemical properties of the analogous compounds without carboxyl groups. On the one hand, complex $[Ru(bpy)_3]^{2+}$ (bpy = 2,2′ -bipyridine) absorbs strongly in the visible region,[65] the ^{3}MLCT excited state, which is populated rapidly with unit efficiency (Φ = 1), is relatively long-lived (0.61 μs in H_2O and 1.00 μs in D_2O),[66] and facilitates energy transfer to $^3O_2$ to form the highly reactive $^1O_2$.[67] In consequence, this compound photocleaves pBR322 plasmid (λ_{irr} > 450 nm) by the type II PDT mechanism.[68] On the other hand, the analogous derivative $[Ru(tpy)_2]^{2+}$ (tpy = 2,2′:6′,2″-terpyridine) exhibits a significantly shorter excited state lifetime of 0.12 ns because the distorted octahedral geometry promotes population of the nonemissive ^{3}MC state.[4] This excited state does not persist long enough to sensitize $^1O_2$ production effectively or cause DNA photodamage. Although the photophysical properties of $[Ru(tpy)_2]^{2+}$ are not very promising, we considered that the behavior in PDT of complex **6**, with a different terpy ligand, should be tested. An important difference with respect to $[Ru(tpy)_2]^{2+}$ is that complex **6** is possibly able to intercalate in the double-stranded DNA. Platinum complexes such as $[PtCl(Phtpy)]^+$ (Phtpy = 4′-phenyl-2,2′:6′,2″-terpyridine) show excellent photophysical properties[69] with enhanced triplet-state population upon excitation, and besides, we have shown that complex **1** exhibits intercalating properties.

The photoinduced DNA interaction abilities of active (**1**) and inactive complexes (**5** and **6**) in the dark were assessed by EM (Figure 8) and AFM (Figure 9) upon irradiation of the samples at λ = 447 nm for different times. Samples treated under dark conditions were used as controls.

Electrophoretic mobility (EM) experiments revealed that, upon photoactivation, complex **6** displayed an enhanced ability to interact with DNA and it generated partially uncoiled forms of pUC18 after irradiation for 40 min (lane 15, Figure 8a). In contrast, 24 h of incubation at 37 °C was required to achieve the effect in the dark (see lane 6, Figure 4a). Under light conditions, a minor photocleavage was evidenced due to the slight intensification of the OC band after irradiation for 2 h (lane 3, Figure 8a). In agreement with the EM data, the AFM image (Figure 9a) shows some broken forms of plasmid and this finding indicates a slight nuclease activity for photoactivated complex **6**.

Upon irradiation, both compounds **5** and **1** showed a marked increase in their capacity for DNA cleavage compared to treatments in the dark according to the EM and AFM data. Thus, for both compounds, the conversion of supercoiled DNA (form CCC) to relaxed open circular DNA (form OC) (lane 3, Figure 8b and c) was observed upon irradiation in a time-dependent manner, although **1** failed to promote the complete conversion of CCC to OC forms. Besides, a linear DNA form could be detected for **5** (lane 3, Figure 8b). The AFM images show linear DNA forms with some other relaxed open circular forms after incubation with photoactivated complex **1** (Figure 9c), while tiny digested DNA fragments were observed after treatment with photoactivated complex **5** (Figure 9b). Both EM and AFM revealed that, upon photoactivation, complex **5**, inactive in the dark, displayed a higher nuclease activity than **1**.

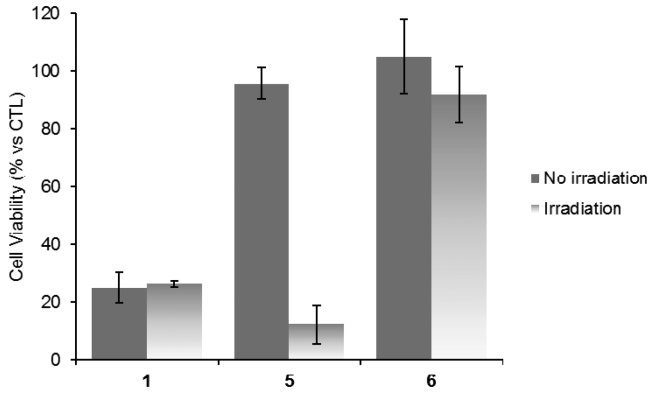

Figure 10. Effect of photoactivation on the cytotoxic activity of **1**, **5**, and **6**. PC-3 cells were treated with **6** (100 μM), **5** (100 μM), or **1** (5 μM) for 1 h and then irradiated for 1 h with a royal blue LED (840 mW, 700 mA). Nonirradiated cells were included as a control. Cell viability was determined after 48 h of treatment. Bars indicate the mean cell viability and the standard deviation after each treatment.

Considering this increase in the nuclease activity of complexes **1**, **5**, and **6** after irradiation, we decided to explore the effect that photoactivation had on their cytotoxicity. To this end, PC-3 cells were incubated with complexes **1**, **5**, and **6** for 1 h at the indicated concentrations (Figure 10), according to the corresponding IC_{50}, and then irradiated for 1 h. The cell viability was determined 48 h later. It can be seen from Figure 10 that irradiation did not alter the cytotoxicity of complexes **1** and **6**. Interestingly, for compound **5**, the cell viability was significantly reduced from 95.7 ± 5.4 to 12.3 ± 6.6 μM after irradiation, which corresponds to a phototoxic index (PI) of 7.8 relative to the nonirradiated experiment with the same incubation time. These results reveal the potential of **5** as a prodrug, with cytotoxic activity only after

DOI: 10.1021/acs.inorgchem.7b01178
Inorg. Chem. 2017, 56, 13679−13696

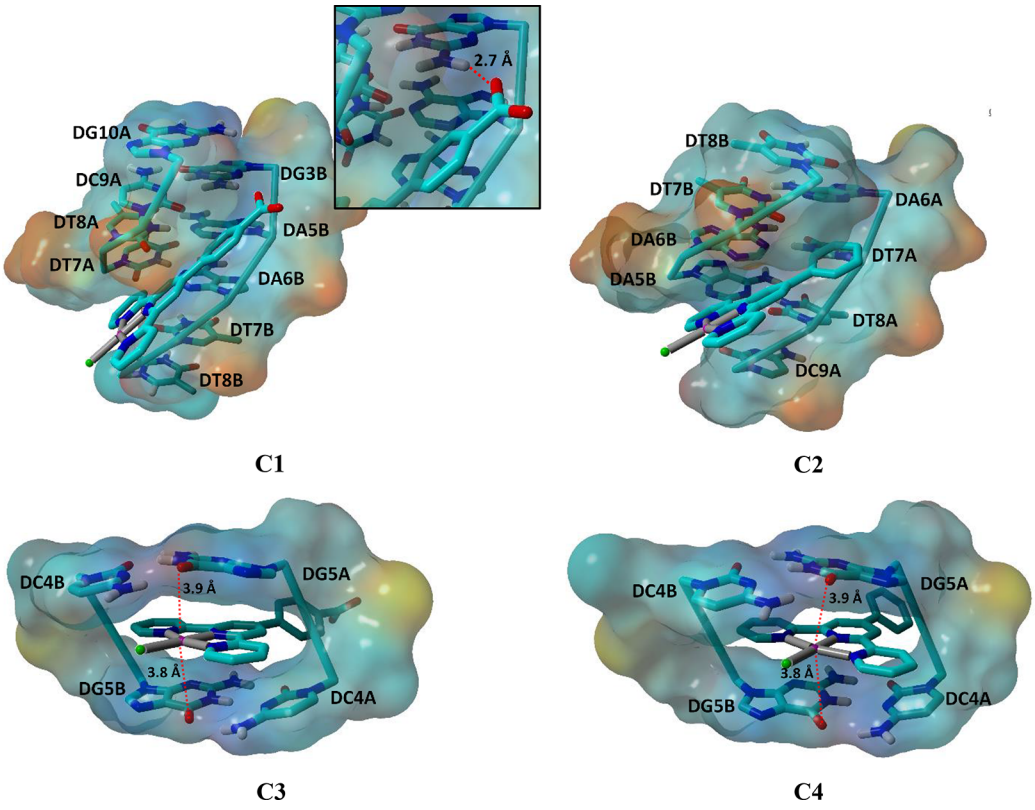

Figure 11. Docking poses obtained for ligands **1** and **1′** using 1BNA (**C1** and **C2**) and 1XRW (**C3** and **C4**) as templates. Only deoxynucleotides involved in noncovalent contacts with the ligands are labeled. For clarity, deoxyribose, phosphate groups, and nonpolar hydrogens have been omitted. The van der Waals surfaces of the deoxynucleotides are shown, and they are the same color as the atoms that contribute to them. Red dotted lines represent the following: the H-bond between the amino group of DG3B and the carboxylate group of ligand **1** for **C1** (see inset) or the distance between Pt and oxygen atoms of DG5A and DG5B for **C3** and **C4**.

photoinduction, which is probably related to the marked increase in its nuclease activity under light.

Computational Studies. As stated, drugs that interact in a noncovalent way with DNA are mostly groove binders and/or DNA intercalators. The groove-binding mode is facilitated through van der Waals and hydrogen bonding interactions, thereby inhibiting the regular function of DNA.[70] Otherwise, intercalators contain planar heterocyclic groups that stack between adjacent DNA base pairs through $\pi-\pi$ stacking interactions to induce strong structural perturbations in DNA.[71]

It has been proposed that the protocol to distinguish between DNA intercalators from DNA groove binding ligands without any prior knowledge of the binding modes is to perform docking studies using different DNA templates both with and without preformed intercalation gaps followed by molecular dynamics calculations.[72]

Complex **1** was chosen for this study due to its experimental cytotoxicity and interaction with DNA. Although it has been demonstrated experimentally that derivative **1** is able to intercalate in the double-stranded DNA, both types of DNA templates were considered and the molecular dynamics calculations were also applied as explained below to justify the reasons of the obtained experimental binding mode. The chlorido complex **1** was used and not the aqua species due to the lack of hydrolysis experimentally observed. It was considered reasonable that the deprotonated carboxyl form of **1** was the most abundant species at the pH of the experimental DNA interaction studies (pH 7.4).

Molecular Docking Studies. Molecular docking studies are a well-documented computational tool to understand the drug–DNA interactions in rational drug design and also in mechanistic studies by placing a small molecule into the binding site of the target specific region of the DNA, mainly with reference to noncovalent interactions. AutoDock is one of the most widely used docking software packages because its empirical free energy scoring function is efficient in evaluating ligand:DNA interactions and binding modes, at least in a qualitative way.[73]

1 and **1′** (analogue of **1** without the carboxylate group) were used as ligands in molecular docking studies to form aggregates formed after their interaction with DNA models that will be called complexes. The structures were previously optimized using the B3LYP functional and were docked with two DNA fragments of B-DNA: the dodecamer D(CGCGAATTCGCG)$_2$ (PDB ID: 1BNA) and the octamer d(CCTCGTCC)$_2$ 5′-D(CCTCGTCC)-3′/5′-D(GGACGAGG)-3′ (PDB ID: 1XRW). The crystal structures were retrieved from the RCSB Protein Data Bank (http://www.rcsb.org./pdb) and used as receptors (Figure S16). The structure of 1XRW contains a preformatted intercalation gap occupied by an acridine urea derivative, which was removed to obtain the bare receptor. All of the water molecules were also removed.

Receptor 1BNA. The molecular docking studies using 1BNA as the receptor showed that the most energetically favorable binding site for ligands **1** and **1′** corresponds to a binding to in the minor groove (**C1** and **C2** in Figure 11). No other binding modes were obtained in the docking calculation.

DOI: 10.1021/acs.inorgchem.7b01178
Inorg. Chem. 2017, 56, 13679–13696

Table 2. Intramolecular Terms of the Scoring Function of AutoDock for the Docked Poses in kcal/mol

receptor	ligand	complex	binding energy	VdW+HB+D energies[a]	electrostatic energy	torsional energy
1BNA	**1**	**C1**	−9.60	−9.90	−0.52	0.82
	1′	**C2**	−9.66	−9.31	−0.62	0.27
1RXW	**1**	**C3**	−7.15	−8.59	0.62	0.82
	1′	**C4**	−8.26	−8.58	0.05	0.27

[a]vdW + H-bond + desolvation.

It is well-known that small molecules preferentially interact with the minor groove due to the lower level of steric interference when compared to larger molecules.[74] Additionally, the typical minor-groove binding molecules have aromatic rings connected by single bonds, which impart appropriate torsional flexibility. From this point of view, ligands **1** and **1′** seem to fit this profile.

Concerning the energy evaluation of the docking processes obtained, the resulting binding energies for **C1** and **C2** were −9.60 and −9.66 kcal/mol, respectively (Table 2). These values are in the same range as those found in other related Pd(II) and Pt(II) coordination compounds docked with DNA.[75,76] This energy is a combination of three primary factors, among which the van der Waals + H-bond + desolvation term plays the most important role, with energies of −9.90 and −9.31 kcal/mol for **C1** and **C2**, respectively. The energetic difference in this term obtained for these two complexes reflects the presence of an intermolecular hydrogen bond between the carboxylate group of **1** and the amino group of DG3B (2.7 Å, **C1** in Figure 11). This amino group is the only H-bond donor group oriented toward the minor groove. The less favorable electrostatic energy component obtained for **C1** is related to the repulsive electrostatic interaction of the carboxylate group of **1** with the phosphate groups of the DNA framework. Torsional energies show noteworthy changes (0.82 and 0.27 kcal/mol for **C1** and **C2**, respectively) because the presence of the carboxylate group gives an additional routable bond in the former. This factor approximately neutralizes the favorable effect of the hydrogen bond in **C1** (Table 2).

The ligand and DNA residue contacts for **C1** and **C2** are shown in Figure 11. In both complexes, the interactions occur within a region that is rich in adenine (DA) and thymine (DT) deoxyribonucleotides and thus the aromatic rings of both ligands are embedded in this region, while the carboxylate group of **1** is hydrogen bonded to the DG3B base. These observations are related to the fact that the DNA minor groove is narrower in A−T- than in G−C-rich sequences. Therefore, the aromatic rings of **1** and **1′** fit better into the A−T-rich region to make optimal van der Waals contacts with the deoxyribonucleotides. On the other hand, the presence of a guanine base is necessary to build the intermolecular hydrogen bond with the carboxylate group of ligand **1**, which causes a small shift of this ligand toward a G−C region. It can be concluded that ligands with groups capable of accepting H-bonds from the guanine amino group offer a way of increasing the number of binding sites in regions of the minor groove that are rich in G−C.

Receptor 1XRW. Using 1XRW as a receptor, ligands **1** and **1′** dock in the intercalation gap (**C3** and **C4** in Figure 11) and no other binding mode was obtained in these docking calculations. The values of the different docking energy terms are provided in Table 2.

The energy values of the van der Waals + H-bond + desolvation term for **C3** and **C4** are similar and less negative than those obtained for **C1** and **C2**. This last fact is related to the significantly lower number of DNA−ligand hydrophobic contacts and van der Waals interactions observed for **C3** and **C4**. Only four deoxyribonucleotides of the 1XRW receptor interact with the ligand: DG5A:DC4B and DC4A:DG5B through $\pi-\pi$ interactions between the terpyridine moiety of the ligands and aromatic parts of the base pairs (Figure 11). In addition to the presence of the carboxyl group in **1**, another factor that contributes to the increase in the repulsive character of the electrostatic energy terms, when compared to those obtained using 1BNA as the receptor (Table 2), are the interactions between the negatively charged nitrogen atoms of the terpyridine moiety and oxygen and nitrogen atoms of the nucleobases. Despite the differences in the values of the components of the scoring functions, the binding energy values for the four complexes (**C1**−**C4**) do not show large differences.

Binding Modes Refined by Molecular Dynamics Simulations. MDS were used to determine the stability of each complex obtained by docking calculations and to predict the most consistent binding modes. The strength of the combination of docking calculations and MDS lies in their complementary capabilities. Docking techniques are used to explore the huge conformational space of ligands by considering the receptor in a rigid way. In contrast, MDS can treat both ligand and receptor in a flexible manner, thus allowing an induced fit of the binding site around the introduced ligand and the exploration of different conformations of the receptor-ligand complex, which can generate a reliable ranking of the final complexes. In addition, the effect of explicit water molecules in a biological medium is also considered in this kind of calculation.[77]

The complexes obtained (**C1**−**C4**) from the docking calculation were used as starting structures to perform MDS. To examine conformational variations in the complexes during the simulations, the root-mean-square deviations (RMSDs) of the time-dependent atomic positions of complexes were calculated with respect to the starting one. The RMSD trajectories for the backbone atoms (all atoms, in red) and for the heavy atoms (C, N, O, Cl, and Pt, in blue) of the complexes as a function of the simulation time (100 ns) are shown in Figure S17. The average RMSD values for these trajectories were about 2.9 and 2.6 Å for **C1** and 3.4 and 6.6 Å for **C2**, respectively. Both trajectories are quite similar in **C1** but not in **C2** where a large jump is observed at 40 ns on the heavy atoms trajectory. This fact is related to the observed release of ligand **1′** from the binding site during the MDS of **C2**. The lack of a hydrogen bonding interaction between ligand **1′** and 1BNA, along with the structural fluctuations of the backbone atoms due to the molecular thermal energy, induces changes in the ligand−receptor interaction energy, which in turn alters the binding affinity and leads to the release of ligand **1′** from the minor groove. The larger stabilization (small RMSD values) that is observed in **C1** during the simulation time mainly arises due to the existence of the intermolecular hydrogen bond between the ligand and the G3B base. However, the calculated average structure of **C1** (**C1***) obtained for all of the MDS reveals a significant decrease in the number of residue contacts between 1BNA and ligand **1** over time (compare the number of

DOI: 10.1021/acs.inorgchem.7b01178
Inorg. Chem. 2017, 56, 13679−13696

nucleobase residues for **C1** and **C1*** in Figures 11 and S18, respectively). Thus, the binding affinity of this ligand in **C1** decreases over time. All of these results suggest that the groove-binding mode is not the preferential interaction for ligands **1** and **1′** with DNA.

As far as **C3** and **C4** are concerned, the average RMSD values obtained for the backbone and heavy atom trajectories were about 2.4 and 2.5 Å for **C3** and 2.4 and 2.2 Å for **C4**, respectively. The observed trajectories reflect some noticeable fluctuations for **C3** and **C4** (Figure S17), but the ligands remain intercalated in the gap until the end of the simulation, with the distance from the terpyridine moiety to the two base pairs of the binding region remaining almost constant during the simulation time. Visual inspection (not shown) of the structures over MDS reveals that the observed fluctuations in the trajectories are related to the rotation of the phenyl group and a wagging movement on a plane parallel to those of the base pairs of the cavity gap. Thus, the distances between the platinum and oxygen atoms of the bases G5A and G5B, with values of 3.8 and 3.9 Å, respectively, are the same for complexes **C3** and **C4** (Figure 11). These distances remain virtually unchanged during the simulation, and their values (Figure S15) were 3.6 and 3.8 Å, respectively, for the average structures **C3*** and **C4***, reflecting the huge stability of these complexes.

It can be concluded that, although the intercalation of the ligand gives rise to some structural modifications of the base pair of the binding region, the ligand is not pulled out of the gap during the MDS and the number of contacts and the types of intermolecular interactions remain constant. These results suggest that intercalation is a more favorable binding mode than groove binding for ligands **1** and **1′**. This is in agreement with the experimental data for complex **1** of EM, viscosimetry, and fluorescence emission spectroscopy already discussed and supports this action mode as a reasonable way of the observed biological action.

CONCLUSIONS

The Pt(II) and Ru(II) derivatives containing ligands with pendant carboxyl groups exhibit different behavior against DNA and also in cytotoxicity studies with four cancer cell lines. The Ru−arene complexes **3** and **4** and the Ru−polypyridyl complex **5** did not show any interaction with DNA and failed to induce any cytotoxicity against cancer cells. Complex **2**, in a similar way to the non-carboxyl acid counterpart, presumably interacts covalently with DNA, but cytotoxicity was not observed in the studied cell lines. Complexes **1** and probably **6** have the ability to intercalate in the DNA double helix, a fact that may be related to the presence of the π-extended ligand cptpy. However, their cytotoxicity is clearly different. While **1** reduces the cell viability in the lines tested with IC_{50} values similar to those of cis-Pt for the PC-3 line, compound **6** can be considered as essentially noncytotoxic in these cell lines.

Docking studies on complex **1** (carboxyl-deprotonated) or its counterpart without the carboxylate group (**1′**) either with receptor 1BNA or 1XRW reflected a binding in the minor groove or an intercalation binding mode, respectively. MDS studies concluded that the binding affinities of the complexes in the minor groove decreased over time, especially in the case of **1′** that is pulled from the minor groove, while **1** is retained due to an intermolecular hydrogen bond established with the carboxyl acid group. However, these dynamic studies reflected a higher stability of the intercalated complexes, confirming that the intercalation is the most favorable binding mode for both derivatives.

Concerning PDT studies, after irradiation at λ = 447 nm, derivatives **1** and **6** increased interaction with DNA—especially **1**, which markedly increased nuclease activity. However, an improvement in their cytotoxic properties after irradiation was not observed. In accordance with the promising photophysical properties of the $[Ru(bpy)_3]^{2+}$ complex, the most interesting behavior was found for **5**. After irradiation, significant DNA photocleavage is observed along with a marked increase in its cytotoxic activity, a fact that makes complex **5** a potential prodrug of interest in PDT.

In conclusion, considering the results of the experimental studies, complexes **1** and **5** (the latter in the presence of light) are valuable candidates for conjugation to peptide carriers whose receptors are overexpressed in cancer cells, in particular in prostate cancer cells. This strategy might increase the selectivity and also the intracellular accumulation, thus potentially increasing the anticancer activity. Experiments with this aim are underway in our laboratories.

EXPERIMENTAL SECTION

Physical Methods. All synthetic manipulations were carried out under an atmosphere of dry oxygen-free nitrogen using standard Schlenk techniques. Solvents were distilled from the appropriate drying agents and degassed before use. Elemental analyses were performed with a Thermo Quest FlashEA 1112 microanalyzer. The analytical data for the new complexes were obtained from crystalline samples where possible. IR spectra were recorded on a Shimadzu IR Prestige-21 IR spectrophotometer equipped with a Pike Technologies ATR, on a Nicolet Impact 410 spectrophotometer as KBr pellets, or on a Jasco (650−160 cm^{-1} range) system as Nujol mulls deposited on a polyethylene film. Only relevant bands are collected. Fast atom bombardment mass spectra (FAB MS) (position of the peaks in Da) were recorded with an Autospec spectrometer or a Thermo MAT95XP mass spectrometer with a magnetic sector. NMR spectra were recorded at 298 K (unless otherwise stated) on a Varian Unity Inova 400 or on a Varian Innova 500 spectrometer. ^1H and $^{13}C\{^1H\}$ chemical shifts were internally referenced to TMS via the residual ^1H and ^{13}C signals of $CDCl_3$ (δ = 7.26 ppm and δ = 77.36 ppm) and DMSO-d_6 (δ = 2.50 ppm and δ = 29.84 and 206.26 ppm), according to the values reported by Fulmer et al.[78] Chemical shift values are reported in ppm and coupling constants (J) in Hz. The splitting of proton resonances is defined as s = singlet, d = doublet, t = triplet, sept = septet, m = multiplet, bs = broad singlet. C_q = quaternary carbon. The ^{31}P resonances were referenced to 85% H_3PO_4 at 0 ppm. 2D NMR spectra were recorded using standard pulse−pulse sequences: COSY (COrrelation SpectroscopY), NOESY (Nuclear Overhauser Enhancement SpectroscopY), HMQC (Heteronuclear Multiple Quantum Coherence), HMBC (Heteronuclear Multiple Bond Correlation). The probe temperature (±1 K) was controlled by a standard unit calibrated with a methanol reference. All NMR data processing was carried out using MestReNova version 6.1.1. In the $^{13}C\{^1H\}$ NMR resonances of complexes **3** and **4**, all of the couplings are with phosphorus.

The light source for the photoactivation assays was a royal blue LED (840 mW, 700 mA) with a λ_{max} at 447 nm (Luxeon star led, Ontario (Canada)). Fluorescence spectra were recorded on a JASCO FP-6200 spectrofluorimeter.

Materials and Synthesis. Reagents and solvents used were of commercially available reagent quality unless otherwise stated. Solvents were purchased from SDS; calf thymus-DNA (CT DNA) type XV, EDTA (ethylenediaminetetracetic acid), and Tris−HCl (tris(hydroxymethyl)-aminomethane−hydrochloride) were obtained from Sigma (Madrid, Spain). The concentration of CT-DNA was determined from its absorption intensity at 260 nm with a molar extinction coefficient of 6600 M^{-1} cm^{-1}. The pUC18 plasmid DNA used in the AFM and EM studies was purchased from Thermo Fisher Scientific (Waltham, MA,

DOI: 10.1021/acs.inorgchem.7b01178
Inorg. Chem. 2017, 56, 13679−13696

USA). Ultrapure agarose was obtained from ECOGEN (Barcelona, Spain); HEPES (*N*-2-hydroxyethyl piperazine-*N*′-2-ethanesulfonic acid) was obtained from ICN (Madrid). Ru and Pt salts were purchased from JOHNSON MATTHEY PLC. Cacodylic acid 98%, 2,2′:6′,2″-terpyridine, 2,2′-bipyridine, 4-carboxybenzaldehyde, 2-acetylpyridine, and 4,4′-dimethyl-2,2′-bipyridine were purchased from Acros Organics. 3-(4,5-Dimethylthiazol-2-yl)-2,5-diphenyltetrazolium bromide (MTT), dimethyl sulfoxide (DMSO), propidium iodide (PI), SeO_2, and silver salts ($AgNO_3$, $AgCF_3SO_3$, $Ag_2C_2O_4$) were obtained from Sigma-Aldrich. NaOH, Celite and NH_4OH, HCl solutions were purchased from Fisher Scientific. $[Ru(p\text{-cym})Cl_2]_2$ was prepared as reported in the literature.[79]

Synthesis of Ligands and Complexes. *4′-(4-Carboxyphenyl)-2,2′:6′,2″-terpyridine, cptpy.* 4-Carboxybenzaldehyde (1 g, 6.7 mmol) was dissolved in absolute ethanol (20 mL) with stirring for 5 min. 2-Acetylpyridine (1.4 mL, 12.5 mmol), concentrated NH_4OH (1 mL), and a solution of NaOH (0.45 g in 1 mL of H_2O) were consecutively added. The reaction mixture was stirred at 45 °C for 48 h, and the formation of a white precipitate was observed. The solid was filtered off and washed with CH_2Cl_2 (3 × 4 mL) and with a 1:1 mixture of cold methanol:H_2O (3 × 5 mL). A beige colored solid was obtained after drying and air was passed through for 2 h. The product obtained at this stage was the corresponding Na salt of the compound. The crude product was suspended in CH_3OH/H_2O (80:20), stirred, and sonicated at 35 °C until complete dissolution. The solution was acidified to pH 2 with 1 M HCl. The resulting white solid was filtered off and dried by vacuum filtration after rinsing with cold water. This compound was used without further purification (1.94 g, 82%). ^{1}H NMR (500 MHz, DMSO-d_6, 25 °C, TMS): δ = 8.76 (d, ^3J = 5.3 Hz, 2H; $H^{6,6''}$), 8.73 (s, 2H; $H^{3',5'}$), 8.66 (d, ^3J = 8.1 Hz, 2H; $H^{3,3''}$), 8.14 (d, ^3J = 8.4 Hz, 2H; $2H^{meta}$), 8.03 (m, 4H; $H^{4,4''}$ + $2H^{ortho}$), 7.53 (m, 2H; $H^{5,5''}$) ppm. ^{1}H NMR of the Na salt (500 MHz, D_2O, 25 °C, TMS): δ = 7.93 (d, J = 4.9 Hz, 2H; $H^{6,6''}$), 7.63 (d, J = 7.8 Hz, 2H; H^{meta}), 7.47 (t, J = 5.9, 2H, $H^{4,4''}$), 7.33 (s, 2H, $H^{3',5'}$), 7.32 (d, J = 5.9, 2H, $H^{3,3''}$), 7.12 (d, 7,8 Hz, 2H, H^{ortho}), 7.02 (dd, J = 7.3, 5.9 Hz, 2H, $H^{5,5''}$) ppm.

4′-Methyl-2,2′-bipyridine-4-carboxylic acid, cmbpy. A mixture of SeO_2 (0.7227 g, 6.5 mmol) and 4,4′-dimethyl-2,2′-bipyridine (1 g, 5.42 mmol) in 1,4-dioxane (65 mL) was heated under reflux for 24 h with vigorous stirring. The resulting mixture was filtered hot through a Celite pad. The yellow liquor was evaporated to dryness. A cream-colored residue was obtained, and this was suspended in ethanol (35 mL). An aqueous solution of $AgNO_3$ was added (1.014 g, 5.96 mmol) in 10 mL of water, and the solution was stirred as 1 M aqueous NaOH (25 mL) was added dropwise (1 g of NaOH in 25 mL of water). A black precipitate of Ag_2O formed. The mixture was vigorously stirred overnight. The corresponding volume of ethanol was removed on a rotary evaporator, and the remaining aqueous solution was filtered to remove the silver residue. The solid residue was washed with 1.3 M NaOH (3 × 7 mL) and then with water (2 × 10 mL). The washings were added to the filtrate, and the pH was adjusted to 3.5 with HCl (0.1 M). The resulting white precipitate was filtered off and characterized by ^{1}H NMR as a mixture of the desired monocarboxyl (80%) and dicarboxyl derivatives (20%). The monocarboxyl compound was separated by Soxhlet extraction using acetone as solvent (300 mL in a 500 mL round-bottomed flask) for 3 d. Yield 0.866 g, 72%.

[PtCl(cptpy)]Cl, 1. In a 100 mL round-bottomed flask, 1 equiv of conc. HCl (37%, 10 μL, 0.113 mmol) was added to a suspension of $K_2[PtCl_4]$ (47.0 mg, 0.113 mmol) and cptpy (40.0 mg, 0.113 mmol) in deoxygenated DMF (20 mL). Partial dissolution of the precipitate occurred. The mixture was heated at 65 °C for 24 h. During this time, a pale orange precipitate formed. The mixture was cooled to room temperature, and the solid was filtered off and rinsed with cold water (3 × 5 mL) and finally dried with air for 4 h. Yield: 37.9 mg, 76%. Complex **1** is insoluble in most organic solvents and in water but is soluble in DMSO. Elemental analysis (%) calcd for $C_{22}H_{15}Cl_2N_3O_2Pt\cdot H_2O$ (601.94): C 42.7, H 2.44, N 6.78; Found: C 42.6, H 2.91, N 6.93. ^{1}H NMR (500 MHz, DMSO-d_6, 25 °C, TMS): δ = 9.03 (d, J = 7.8 Hz, 2H, $H^{3,3''}$), 8.95 (s, 2H, $H^{3',5'}$), 8.93 (d, J = 4.9 Hz, 2H; $H^{6,6''}$), 8.44 (t, J = 7.8 Hz, 2H; $H^{4,4''}$), 8.19 (d, J = 7.8 Hz, 2H; H^{meta}), 8.15 (d, J = 7.8 Hz, 2H; H^{ortho}), 7.87 (t, J = 5.4 Hz, 2H; $H^{5,5''}$) ppm. ^{13}C NMR (500 MHz, DMSO-d_6, 25 °C, TMS): δ = 167.57 (COOH), 150.19 (C_q), 147.09 ($C^{3,3''}$ or $C^{3',5'}$), 143.23 ($C^{4,4''}$), 140.98 (C_q), 132.70 (C_q), 130.89, 128.29 (C^{ortho} and C^{meta}), 127.07 ($C^{5,5''}$), 124.01 ($C^{3,3''}$ or $C^{3',5'}$), 121.21 ($C^{6,6''}$) ppm. IR (ATR): $\overline{\nu}$ = 3450 ν(O—H); 3080−3070 ν(C—H); 1720 ν(C═O); 1613 and 1560 ν(C═N) and ν(C═C); 1270 δ(C—H); 758 δ(C—H) cm^{-1}.

[PtCl$_2$(cmbpy)], 2. $K_2[PtCl_4]$ (100 mg, 0.241 mmol), cmbpy (51.57 mg, 0.241 mmol), and conc. HCl (37%, 20 μL, 0.241 mmol) were mixed in deoxygenated water (20 mL). The mixture was heated at 65 °C for 15 h to give a yellow precipitate, which was filtered off and rinsed with cold water (3 × 5 mL). The solid was dried in air for 4 h. Yield: 91.4 mg, 79%. Complex **2** is insoluble in most organic solvents and in water but soluble in DMSO. Elemental analysis (%) calcd for $C_{12}H_{10}Cl_2N_2O_2Pt$ (480.22): C 30.01, H 2.10, N 5.83; Found: C 29.65, H 2.28, N 5.71. ^{1}H NMR (500 MHz, DMSO-d_6, 25 °C, TMS): δ = 14.5 (bs, COOH); 9.63 (d, J = 6.0 Hz, 1H; $H^{6'}$), 9.24 (d, J = 6.0 Hz, 1H; H^6), 8.78 (s, 1H; H^3), 8.68 (s, 1H; $H^{3'}$), 8.15 (d, J = 6.0 Hz, 1H; $H^{5'}$), 7.67 (d, J = 6,0 Hz, 1H; H^5), 2.49 (s, 3H; Me^4) ppm. ^{13}C NMR (500 MHz, DMSO-d_6, 25 °C, TMS): δ = 165.52 (COOH), 158.74 ($C^{4'}$), 156.46 ($C^{2'}$), 153.87 (C^2), 150.20 ($C^{6'}$), 148.39 (C^6), 142.24 (C^4), 129.21 (C^5), 127.74 ($C^{3'}$), 126.40 (C^3), 124.05 ($C^{5'}$), 21.81 (CH_3) ppm. IR (ATR): $\overline{\nu}$ = 3432 ν(O—H); 3090−3071 ν(C—H); 1724 ν(C═O); 1613, 1558, and 1553 ν(C═N) and ν(C═C); 1250 δ(C—H); and 760 δ(C—H).

[Ru(p-cym)Cl$_2$(dpb)], 3. $[Ru(p\text{-cym})Cl_2]_2$ (100 mg, 0.16 mmol) was dissolved in dichloromethane (20 mL) in a Schlenk tube. The solution was stirred, and the ligand dpb (100 mg, 0.33 mmol) was added. The solution was stirred for 24 h at r.t. The solvent was evaporated under vacuum, and the solid was washed with hexane and dried under vacuum. The complex was dark orange. Yield: 179 mg, 90%. Complex **3** is soluble in acetone, dichloromethane, and methanol, partially soluble in ethanol, and insoluble in water. Elemental analysis (%) calcd for $C_{29}H_{29}Cl_2O_2PRu$ (612.50): C 56.87; H 4.77; Found: C 56.73; H 4.90. ^{1}H NMR (400 MHz, $CDCl_3$, 25 °C): δ = 8.00 (dd, $^3J_{HH}$ = 8.5 Hz, $^4J_{PH}$ = 2.1 Hz, 2H, $H^{3',5'}$-dpb), 7.93 (m, 2H, $H^{2',6'}$-dpb), 7.82 (m, 4H, $H^{ortho\text{-}Ph}$-dpb), 7.42 (m, 6H, $H^{meta,para\text{-}Ph}$-dpb), 5.23 (d, J = 6.2 Hz, 2H, $H^{2,6}$-cym), 4.99 (d, J = 5.3 Hz, 2H, $H^{3,5}$-cym), 2.86 (sept, J = 13.8 Hz, 1H, H^7-cym), 1.87 (s, 3H, H^{10}-cym), 1.12 (d, J = 7.0 Hz, 6H, $H^{8,9}$-cym) ppm. ^{1}H NMR (400 MHz, DMSO-d_6, 25 °C): δ = 13.12 (s, 1H, −COOH-dpb), 7.87 (m, 2H, $H^{3',5'}$-dpb), 7.76 (m, 2H, $H^{2',6'}$-dpb), 7.44 (m, 10H, $H^{ortho,meta,para\text{-}Ph}$-dpb), 5.34 (d, J = 6.2 Hz, 2H, $H^{2,6}$-cym), 5.26 (d, J = 6.2 Hz, 2H, $H^{3,5}$-cym), 2.51 (m, 1H, H^7-cym), 1.77 (s, 3H, H^{10}-cym), 0.94 (d, J = 6.9 Hz, 6H, $H^{8,9}$-cym) ppm. ^{13}C{^{1}H}-NMR (101 MHz, $CDCl_3$, 25 °C): δ = 170.54 (s, 1C, COOH-dpb), 140.38 (d, J = 43.6 Hz, 1C, $C^{1'}$-dpb), 134.57 (d, J = 9.2 Hz, 2C, $C^{2',6'}$-dpb), 131.47 (d, J = 9.5 Hz, 4C, $C^{ortho\text{-}Ph}$-dpb), 133.31 (d, J = 45.4 Hz, 2C, C^{ipso}-dpb), 130.78 (d, J = 2.4 Hz, 2C, $C^{para\text{-}Ph}$-dpb), 130.48 (d, J = 2.3 Hz, 1C, $C^{4'}$-dpb), 129.32 (d, J = 10.0 Hz, 2C, $C^{3',5'}$-dpb), 128.39 (d, J = 9.9 Hz, 4C, $C^{meta\text{-}Ph}$-dpb), 111.74 (d, J = 3.6 Hz, 1C, C^1-cym), 96.49 (s, 1C, C^4-cym), 89.08 (d, J = 3.1 Hz, 2C, $C^{3,5}$-cym), 87.52 (d, J = 5.5 Hz, 2C, $C^{2,6}$-cym), 30.46 (s, 1C, C^7-cym), 22.02 (s, 2C, $C^{8,9}$-cym), 17.96 (s, 1C, C^{10}-cym) ppm. ^{31}P{^{1}H}-NMR (162 MHz, $CDCl_3$, 25 °C): δ = 26.26 (s, 1P, dpb) ppm. ^{31}P{^{1}H}-NMR (162 MHz, DMSO-d_6, 25 °C): δ = 25.73 (s, 1P, dpb) ppm. FT-IR (KBr, cm^{-1}): $\overline{\nu}$ = 3058 ν(C_{sp2}—H), 2962 ν(C_{sp3}—H), 1716 ν_{as}(COO), 1599, 1435 ν(P—C), 1395 ν_s(COO), 1093, 749 δ(C_{arom}—H), 698 δ(C_{arom}—H), 539 (dpb), 519 (dpb) cm^{-1}. FT-FIR (Nujol, cm^{-1}): $\overline{\nu}$ = 354, 282 ν(Ru—Cl), 227 ν(Ru—P). Mass FAB+ (m/z): 612 ([M − H]$^+$), 577 ([M − Cl]$^+$), 541 ([M − 2Cl]$^+$), 442 ([M − cym − Cl]$^+$), 407 ([M − cym − 2Cl]$^+$), 306 ([M − dpb]$^+$), 271 ([M − Cl − dpb]$^+$).

[Ru(p-cym)(ox)(dpb)], 4. $[Ru(p\text{-cym})Cl_2]_2$ (100 mg, 0.16 mmol) was dissolved in methanol (20 mL). The solution was stirred, and $Ag_2C_2O_4$ (99 mg, 0.33 mmol) was added. The solution was protected from light and stirred for 2 h. The mixture was filtered through Celite. Dpb (327 mg) was added to the solution, and this was stirred for 24 h at r.t. The solution was concentrated under a vacuum, and a solid was precipitated by the addition of diethyl ether. The solid was filtered off, washed with diethyl ether, and then dried under vacuum. The resulting solid is yellow colored. Yield: 103 mg, 50%. Complex **4** is soluble in DMSO, scarcely soluble in acetone and dichloromethane, and insoluble in water. Elemental analysis (%) calcd for $C_{31}H_{29}O_6PRu\cdot H_2O$

DOI: 10.1021/acs.inorgchem.7b01178
Inorg. Chem. 2017, 56, 13679−13696

(629.62): C 57.49; H 4.82; Found: C 57.57; H 4.77. ^{1}H NMR (400 MHz, DMSO-d_6, 25 °C): δ = 13.23 (s, 1H, H^{-COOH}-dpb), 7.94 (dd, J_{HH} = 8.4 Hz, $^{3}J_{PH}$ = 1.9 Hz, 2H, H$^{3',5'}$-dpb), 7.49 (m, 12H, H$^{Ph,2',6'}$-dpb), 5.71 (d, J = 6.2 Hz, 2H, H^{2,6}-cym), 5.40 (d, J = 6.1 Hz, 2H, H^{3,5}-cym), 2.48 (m, 1H, H^{7}-cym), 1.81 (s, 3H, H^{10}-cym), 1.12 (d, J = 6.9 Hz, 6H, H^{8,9}-cym) ppm. ^{13}C{^{1}H}-NMR (101 MHz, DMSO-d_6, 25 °C): δ = 163.71 (s, 2C, C^{ox}), 161.43 (s, 1C, COOH-dpb), 133.99 (d, J = 10.5 Hz), 133.73 (d, J = 9.7 Hz), 131.14 (d, J = 2.9 Hz), 129.05 (d, J = 8.4 Hz), 128.85 (d, J = 9.8 Hz), 106.08 (s, 1C, C^{1}-cym), 97.54 (s, 1C, C^{4}-cym), 87.79 (d, J = 3.6 Hz, 2C, C^{3,5}-cym), 86.67 (d, J = 3.2 Hz, 2C, ^{2,6}-cym), 30.28 (s, 1C, C^{7}-cym), 21.76 (s, 2C, C^{8,9}-cym), 17.23 (s, 1C, C^{10}-cym) ppm. The assignation of signals in the aromatic region has not been done due to the low quality of the spectrum. ^{31}P{^{1}H}-NMR (162 MHz, DMSO-d_6, 25 °C): δ = 33.84 (s, 1P, dpb) ppm. FT-IR (KBr, cm^{-1}): $\bar{\nu}$ = 3061 ν(C$_{sp2}$—H), 2965 ν(C$_{sp3}$—H), 1693 ν(C═C), 1669 ν_{as}(COO), 1436 ν(P—C), 1390 ν_{s}(COO), 1245, 1096, 781 δ(C$_{arom}$—H), 697 δ(C$_{arom}$—H), 540 (dpb), 521 (dpb), 496 ν(Ru—O) cm^{-1}. FT-FIR (Nujol, cm^{-1}): $\bar{\nu}$ = 280, 211 ν(Ru—P), 157 cm^{-1}. Mass FAB+ (m/z): 630 ([M + H]$^{+}$), 541 ([M − ox]$^{+}$), 406 ([M − ox − cym]$^{+}$).

[Ru(tpy)(cptpy)](PF$_6$)$_2$, **6**. An excess of AgOTf (117.6 mg, 0.47 mmol) was added to an EtOH/DMF (4:1) solution (20 mL) of [RuCl$_3$(tpy)] (84.7 mg, 0.19 mmol). The mixture, protected from light, was heated at 60 °C for 20 min. The ligand cptpy (67.8 mg, 0.19 mmol) was added, and the resulting solution was heated under reflux for 22 h under a nitrogen atmosphere. The resulting reddish solution was filtered to remove AgCl. The solution was evaporated to dryness, and the resulting solid was dissolved in 20 mL of a mixture of CH$_3$CN/H$_2$O (2:1). A saturated solution of NH$_4$PF$_6$ (350 mg, 2.15 mmol) in water was added to this solution and the mixture was stirred for several hours, during which time a precipitate formed. The suspension was evaporated to a half volume, and the solid was isolated by filtration. This solid was washed once with water, cold EtOH, and finally diethyl ether. The product was obtained as a dark red solid. Yield: 159.7 mg, 86%. Complex **6** is very soluble in DMSO, soluble in acetone, less soluble in CHCl$_3$ or CH$_2$Cl$_2$, and insoluble in apolar organic solvents. Elemental analysis (%) calcd for C$_{37}$H$_{26}$N$_6$O$_2$P$_2$F$_{12}$Ru (977.66): C 45.46; H 2.68; N 8.6; Found: C 45.23; H 2.80; N 8.4. ^{1}H NMR (500 MHz, DMSO-d_6, 25 °C, TMS): δ = 9.53 (d, 2H, H$^{3,3''}$(A)), 9.10 (m, 4H; H$^{3',5'}$(A) + H$^{3',5'}$(B)), 8.84 (m, 2H; 2H$^{3,3''}$(B)), 8.55 (m, 3H; 2H^{meta}(A) + H$^{4'}$(B)), 8.29 (m, 2H; 2H^{ortho}(A)), 8.04 (m, 4H; H$^{4,4''}$(A) + H$^{4,4''}$(B)), 7.54 (m, 2H; H$^{6,6''}$(A)), 7.45 (m, 2H; H$^{6,6''}$(B)), 7.45 (m, 4H; H$^{5,5''}$(A) + H$^{5,5''}$(B)) ppm. * A = cptpy; B = tpy.

X-ray Crystallographic Structure Determination for Ligand Salt [Na(H$_2$O)$_4$]cptpy·H$_2$O, 2·2DMF and 5·acetone. A summary of crystal data collection and refinement parameters is given in Table S2.

Data were collected on a Bruker X8 APEX II CCD-based diffractometer, equipped with a graphite-monochromated Mo Kα radiation source (λ = 0.71073 Å). Data were integrated using SAINT,[80] and an absorption correction was performed with the program SADABS.[81] A successful solution by direct methods provided most non-hydrogen atoms from the E map. The remaining non-hydrogen atoms were located in the alternating series of least-squares cycles and difference Fourier maps.[82] All non-hydrogen atoms were refined with anisotropic displacement coefficients. For **2**·2DMF and **5**·acetone, all hydrogen atoms were included in the structure factor calculations at idealized positions and were allowed to ride on the neighboring atoms with relative isotropic displacement coefficients. The hydrogen atoms of the ligand salt [Na(H$_2$O)$_4$]cptpy·H$_2$O were found in Fourier map and then fixed for their refinement. All of the crystals obtained for complex **5**·acetone were very weakly diffracting and of poor quality, and the data could not be refined properly. After several attempts at crystallization, it was not possible to obtain crystals of better quality. However, the dispositions of the atoms are clear and the structure can be explained.

Electrophoretic Mobility in Agarose Gel. DNA interaction was monitored by agarose gel electrophoresis. The pUC18 plasmid DNA was used at a concentration of 0.5 μg/μL (1512 μM nucleotides; 756 μM bp). Complex stock solutions were prepared freshly in Milli-Q water with 5% DMSO to facilitate the dissolution of compounds. Reactions were performed by mixing 0.5 μL of pUC18 with appropriate aliquots of complex solutions. Cacodylate buffer (0.1 M, pH 6.0) or Tris−EDTA (TE) (Tris−H$_4$edta, tris(hydroxymethyl) aminomethaneethylenediaminetetracetic acid) buffer solution (50 mM NaCl, 10 mM Tris−HCl, 0.1 mM H$_4$edta, pH 7.4) was added to the mixture to give a final volume of 20 μL. The final concentration of pUC18 DNA was 37.8 μM in nucleotides (18.9 μM bp). The samples were incubated at 37 °C for different times depending on the experiment. The reactions were quenched by adding a buffer solution (4 μL) consisting of bromophenol blue (0.25%), xylenecyanole (0.25%), and glycerol (30%). The samples were then subjected to electrophoresis on 0.8% agarose gel in 0.5× TBE buffer (0.045 M Tris, 0.045 M boric acid, and 1 mM EDTA) at 100 V for 1 h 40 min. Finally, the DNA was dyed with an ethidium bromide solution (10 mg/mL in TBE) for 15 min and the DNA bands were visualized on a capturing system (ProgRes CapturePro 2.7). A sample of free DNA was used as a control.

Atomic Force Microscopy (AFM). The pUC18 plasmid DNA at 0.50 μg/μL concentration was used for the experiments. Stock solutions (1 mM) of the complexes in Milli-Q water with 5% DMSO were freshly prepared. Samples (Vf = 40 μL) were prepared by diluting 1 μL of DNA pUC18 and an appropriate aliquot of the complex stock solution in HEPES buffer (*N*-2-hydroxyethylpiperazine-*N*′-2-ethanesulfonic acid, 10 mM MgCl$_2$, pH 7.4) (DMSO final concentration <1%). The different solutions and Milli-Q water were passed through 0.2 μm FP030/3 filters (Schleicher & Schuell GmbH, Germany) to provide a clear background. The resulting solutions were incubated for different times at 37 °C. AFM samples were prepared by placing a drop (3 μL) of DNA solution or DNA−metal complex solution onto freshly cleaved mica (Ashville-Schoonmaker Mica Co., Newport News, VA, USA). After adsorption for 10 s at room temperature, the samples were rinsed for 10 s with deionized water and dried under a stream of compressed argon gas. A Nanoscope III Multimode AFM (Digital Instrumentals, Santa Barbara, CA, USA) was used at CCiT-UB (Centres Científics i Tecnològics, Universitat de Barcelona). The images were obtained in air at room temperature (relative humidity lower than 40%) on areas of 2 × 2 μm^2 and operating in tapping mode at a rate of 1−3 Hz.

Circular Dichroism (CD) Spectroscopy. Compound **1** was dissolved in an aqueous solution (prepared with Milli-Q water) of 5% DMSO (2 mg of compound/5 mL). DMSO was used to facilitate the dissolution of compounds to be evaluated. The stock solution was freshly prepared before use. The samples were prepared by addition of aliquots of the stock solution to the appropriate volume of calf thymus DNA in a Tris−EDTA (TE) buffer solution (pH 7.4) (5 mL). The amount of complex added to the DNA solution was designated as r_i (the input molar ratio of Pt(II) to nucleotide[41]). As a blank, a solution in TE of free native DNA was used. The CD spectra of DNA in the presence or absence of metal complex (DNA concentration 20 μg/mL, molar ratios r_i = 0.10, 0.30, 0.50) were recorded at room temperature, after 24 h of incubation at 37 °C, on a JASCO J-720 spectropolarimeter with a 450 W xenon lamp using a computer for spectral subtraction and noise reduction (Centres Científics i Tecnològics (CCiTUB) Universitat de Barcelona). Each sample was scanned twice in a range of wavelengths between 220 and 330 nm. The CD spectra drawn are the average of three independent scans. The data are expressed as average residue molecular ellipticity (θ) in deg·cm^2 ·dmol^{-1}.

Fluorescence Emission Spectrometry. The fluorescence spectra were recorded at room temperature on a JASCO FP-6200 spectrofluorimeter. Ethidium bromide (EB) was used as a reference to determine the relative DNA-binding properties of compound **1** to calf thymus (CT-DNA). The experiments entailed the addition of compound **1** solutions at final concentrations ranging from 0 to 250 μM to samples containing 50 μM CT-DNA (nucleotide) and 50 μM ethidium bromide in Tris−EDTA (TE) buffer solution (pH 7.4) and 5% DMSO. This resulted in a series of solutions with varying concentrations of compound **1** but with a constant concentration of DNA and EB. The influence of the addition of complex **1** to the EB−DNA mixture was measured by recording the variations of the fluorescence emission spectra with excitation at 500 nm and emission between 530 and 680 nm.

Viscosimetry Studies. Viscosity experiments were carried out with a semimicro Ubbelodhe viscometer immersed in a Julabo ME16G thermostated bath maintained at 25.0 ± 0.1 °C. Solutions of compound **1** (with final concentrations ranging from 5 to 15 μM) in Tris−EDTA

DOI: 10.1021/acs.inorgchem.7b01178
Inorg. Chem. 2017, 56, 13679−13696

(TE) buffer solution (pH 7.4) and 2.5% DMSO were added to a solution of calf thymus DNA (100 μM nucleotide) in cacodylate buffer. Flow times were measured in triplicate with a stopwatch. Data are presented as $(\eta/\eta_0)^{1/3}$ versus the ratio of the complex concentration to DNA, where η is the viscosity of the CT-DNA in the presence of the complex and η_0 is the viscosity of the DNA alone. Viscosity values were calculated from the observed flow time of a solution containing DNA corrected for the flow time of buffer alone (t_0), $\eta = (t - t_0)$. According to Cohen and Eisenberg,[83] the relation between the relative solution viscosity (η/η_0) and contour length (L/L_0) is given by the follow equation: $L/L_0 = (\eta/\eta_0)^{1/3}$, where L denotes the apparent molecular length in the absence of the metal compound.

Cell Lines. The human breast cancer cell line MCF-7, pancreatic cancer cell line CAPAN-1, and prostate cancer cell line PC-3 were obtained from the American Tissue Culture Collection (ATTC, Rockville, MD, USA). Human colon adenocarcinoma CACO-2 cells were obtained from The European Collection of Cell Cultures (ECACC). Cells were maintained in Dulbecco's modified Eagle's medium (DMEM) supplemented with 10% fetal bovine serum and 1% penicillin–streptomycin (GIBCO BRL, Grand Island, NY) at 37 °C in a humidified atmosphere containing 5% CO_2. The cells were passaged two times per week.

Cytotoxicity Assays. The cytotoxic activity of the compounds was determined by the MTT reduction assay as previously described.[20] Complexes were dissolved in DMSO and Milli-Q water to obtain the stock solutions. Aliquots of 4000 MCF-7 or PC3 cells and 7000 CAPAN-1 or CACO-2 cells were seeded onto 96-well plates. 48 h later, the cells were treated for 48 h at 37 °C with the different complexes serially diluted in culture medium at concentrations ranging from 0 to 100 μM (DMSO final concentration in the culture medium <1%). After removal of the treatment, the cells were washed with PBS and incubated for 2 additional hours with 100 μL of fresh culture medium together with 10 μL of MTT (Sigma-Aldrich). The medium was discarded, and DMSO (Sigma-Aldrich) was added to each well to dissolve the purple formazan crystals. Plates were agitated at room temperature for 10 min, and the absorbance of each well was determined on a Multiscan Plate Reader (Synergy 4, Biotek, Winooski, USA) at a wavelength of 570 nm. Three replicates for each complex were used, and all treatments were tested at least in three independent experiments. For each treatment, the cell viability was determined as a percentage of the control untreated cells, by dividing the mean absorbance of each treatment by the mean absorbance of the untreated cells. The concentration that reduces by 50% the cell viability (IC_{50}) was established for each complex using a four-parameter curve fit (Gen5 Data Analysis Software, BioTeck).

Colony Formation Assay. PC-3 cells were seeded in 24-well plates (50 000 cells/well). After 24 h, cells were treated with cisplatin and complex **1** at the corresponding IC_{50} (2.5 and 5.5 μmol/L, respectively) or vehicle alone as a control for 6 and 24 h at 37 °C. Subsequently, cells were washed with PBS, collected with trypsin, and plated at low density (3000 cells in a 360 mm plate). Cells were allowed to divide and form colonies for 7–10 days; colonies were then fixed and stained with 2% methylene blue in 50% ethanol. The number of colonies in each plate was determined using the Alpha Innotech Imaging system (Alpha Innotech, San Leandro, CA).

Annexin V-FITC/Propidium Iodide Flow Cytometric Apoptosis Analysis. Analysis of phosphatidylserine externalization in apoptotic cells was determined by a Vybrant Apoptosis Assay Kit #2 (Molecular probes, Invitrogen, Eugene, OR, USA), according to the manufacturer's instructions. PC-3 cells were seeded in 24-well plates and incubated with cisplatin or complex **1** at 25 μM for 24 h. Cells were then collected and suspended in 100 μL of Annexin V-binding buffer. Five μL of Annexin-V-FITC and 10 μL of propidium iodide were added and incubated 15 min at room temperature in the dark. Flow cytometry analysis was carried out using a FACS-Calibur flow cytometer (Becton-Dickinson, Immunofluorometry Systems, Mountain View, CA, USA) and CellQuestTM software (Becton Dickinson).

Photoactivation Assays. The photoinduced DNA-complex interaction was monitored by agarose gel electrophoresis and atomic force microscopy, as described above, under illuminated conditions provided by a royal blue LED with a λ_{max} at 447 nm. The complexes were irradiated for different times, depending on the experiment. The effect of photoactivated complexes **1**, **5**, and **6** on cell viability was analyzed in PC3 cells. Cells were incubated with the complexes at different concentrations for 1 h and then irradiated for 1 h. The cytotoxic activity (IC_{50} values) was determined after 48 h of treatment, as described above. Samples treated under dark conditions were used as controls. The phototoxic index (PI) was defined as the ratio between IC_{50} in the dark and IC_{50} after light irradiation.

Statistical Analysis. Statistical analysis was performed with SPSS statistical software for Windows (version 15.0; SPSS Inc., Chicago, IL, USA). Quantitative variables were expressed as mean and standard deviation (SD) of at least three independent experiments. The normality of the data was tested using the Shapiro–Wilk test. The normality of the data was tested using the Kolmogorov–Smirnov test. The differences between data with normal distribution and homogeneous variances were analyzed using the parametric Student's t test; otherwise, the nonparametric Mann–Whitney test was applied. A value of $p < 0.05$ was considered significant.

Computational Methods. *Ab Initio Calculations.* First, the molecular structures of the ligands (complex **1** and the analogues without the carboxyl group **1′**) were optimized in the ground state at the DFT level with the B3LYP[84,85] implemented in the Gaussian 09 rev. D.O1 package.[86] Effective core potentials (ECPs) were used to represent the innermost electrons of the Pt atom, while its outer electrons were described with the basis set associated with the SDD pseudopotential and its associated double-ζ basis set[87] complemented with a set of f-polarization functions.[88] The 6-31G(d,p) basis was used for the rest of the atoms in the system.

Full geometry optimization and direct location of stationary points were carried out by means of the Schlegel gradient optimization algorithm[89] by using redundant internal coordinates. The bulk effect of the solvent was calculated, with water as solvent ($\varepsilon = 78.35$), by means of a continuum model (SMD).[90]

Molecular Docking Calculations. Visualization of the docked pose was carried out by using Autodock 4.2 and AutodockTools Software.[91] All of the torsion angles in the small molecules were set free to perform flexible docking, polar hydrogen was added by using the hydrogen module in AutoDock Tools (ADT), and nonpolar hydrogens were merged. Gasteiger charges were assigned for both receptors and ligand molecules. For the Pt atom charge, we applied the charge value obtained from the quantum mechanical calculations because Gasteiger charges are not available for transition metal atoms. Docking was conducted by setting the grid box size at 60 Å × 60 Å × 60 Å along the x, y, and z axes, thereby covering the whole 1BNA with a grid spacing of 0.375 Å. AutoGrid was then run to generate the affinity grid map of the different ligand and receptor atoms. Lamarckian genetic algorithms were used to explore the different ligand conformations with the following settings: a maximum number of 25 000 000 energy evaluations, an initial population of 300 randomly placed individuals, a maximum number of 27 000 generations, a mutation rate of 0.02, a crossover rate of 0.80, and an elitism value (number of top individuals that automatically survive) of 1300 independent ligand conformations were carried out for each ligand. The result with the lowest docking energy analysis in cluster rank 1 was used for further analysis and selected as the initial active/binding conformation. The scoring function of AutoDock[92] is based on the AMBER force field and includes different intermolecular components for the atom–atom interactions as well as an estimate of the conformational entropy loss upon binding. DNA residues making nonbonded contacts with the ligand were obtained with LigPlot+ software.[93]

Molecular Dynamics Simulations. Molecular dynamics simulations (MDS) were performed using the AMBER14 force field implemented in YASARA software.[94,95]

A simulation cell was constructed around a DNA–ligand complexes model with a 8 Å real space cutoff for the Lennard-Jones forces and the direct space portion of electrostatic forces, which were calculated using the particle mesh Ewald method. The pK_a values of the ionizable groups were predicted and assigned protonation states based on pH 7.4 (that fixed in the experiments for the DNA interaction studies). The carboxyl group of ligand **1** was deprotonated, since the pK_a value was determined to be 6.8–6.9. The cell was then filled with water, and the AMBER14

DOI: 10.1021/acs.inorgchem.7b01178
Inorg. Chem. 2017, 56, 13679–13696

electrostatic potential was evaluated for all water molecules; the one with the lowest or highest potential was changed to a sodium or chloride counterion until the cell was neutral. A short steepest descent minimization was done to remove severe bumps, followed by simulated annealing minimizations at 298 K, and the velocities were scaled down every 10 steps out of 500 steps over a total time period of 5 ps to a final temperature of 0 K. We then ran MDS with the AMBER14 force field at 298 K and 0.9% NaCl in the simulation cell for 100 ns.

■ ASSOCIATED CONTENT

Supporting Information

The Supporting Information is available free of charge on the ACS Publications website at DOI: 10.1021/acs.inorgchem.7b01178.

Tables and figures of the crystallographic data including noncovalent interactions and supplementary figures concerning the analysis of compound−DNA interaction and computational studies (PDF)

Accession Codes

CCDC 1551158−1551160 contain the supplementary crystallographic data for this paper. These data can be obtained free of charge via www.ccdc.cam.ac.uk/data_request/cif, or by emailing data_request@ccdc.cam.ac.uk, or by contacting The Cambridge Crystallographic Data Centre, 12 Union Road, Cambridge CB2 1EZ, UK; fax: +44 1223 336033.

■ AUTHOR INFORMATION

Corresponding Authors

*E-mail: angeles.martinez@udg.edu.
*E-mail: anna.massaguer@udg.edu.
*E-mail: gespino@ubu.es.
*E-mail: Felix.Jalon@uclm.es.

ORCID

Marta Planas: 0000-0003-4988-4970
Blanca R. Manzano: 0000-0002-4908-4503
Félix A. Jalón: 0000-0002-6622-044X

Notes

The authors declare no competing financial interest.

■ ACKNOWLEDGMENTS

For the UCLM and UBU groups, this work was supported by the MINECO of Spain (Grant project CTQ2014-58812-C2-1-R, FEDER funds). For the UDG group, the work was supported by the University of Girona (Grant MPCUDG2016/076). This research was also cofinanced by FEDER OP2014-2020 of Junta de Comunidades de Castilla-La Mancha and CTQ2015-70371-REDT.

■ REFERENCES

(1) Ndagi, U.; Mhlongo, N.; Soliman, M. E. Metal complexes in cancer therapy − an update from drug design perspective. *Drug Des., Dev. Ther.* **2017**, *11*, 599−616.

(2) Reedijk, J. Platinum Anticancer Coordination Compounds: Study of DNA Binding Inspires New Drug Design. *Eur. J. Inorg. Chem.* **2009**, *2009*, 1303−1312.

(3) Lippert, B. *Cisplatin Chemistry and Biochemistry of a Leading Anticancer Compound*; Helvetica Chimica Acta/Wiley-VCH: Zurich, Switzerland, 1999.

(4) Knoll, J. D.; Turro, C. Control and utilization of ruthenium and rhodium metal complex excited states for photoactivated cancer therapy. *Coord. Chem. Rev.* **2015**, *282*−*283*, 110−126.

(5) Allison, R.; Cuenca, R.; Downie, G.; Camnitz, P.; Brodish, B.; Sibata, C. Clinical photodynamic therapy of head and neck cancers—A review of applications and outcomes. *Photodiagn. Photodyn. Ther.* **2005**, *2*, 205−222.

(6) Wang, X.; Guo, Z. Targeting and delivery of platinum-based anticancer drugs. *Chem. Soc. Rev.* **2013**, *42*, 202−224.

(7) Allison, R.; Moghissi, K.; Downie, G.; Dixon, K. Photodynamic therapy (PDT) for lung cancer. *Photodiagn. Photodyn. Ther.* **2011**, *8*, 231−239.

(8) Babilas, P.; Schreml, S.; Landthaler, M.; Szeimies, R. M. Photodynamic therapy in dermatology: state-of-the-art. *Photodermatol., Photoimmunol. Photomed.* **2010**, *26*, 118−132.

(9) Schatzschneider, U. Photoactivated Biological Activity of Transition-Metal Complexes. *Eur. J. Inorg. Chem.* **2010**, *2010*, 1451−1467.

(10) Moucheron, C. From cisplatin to photoreactive Ru complexes: targeting DNA for biomedical applications. *New J. Chem.* **2009**, *33*, 235−245.

(11) Gill, M. R.; Thomas, J. A. Ruthenium(II) polypyridyl complexes and DNA—from structural probes to cellular imaging and therapeutics. *Chem. Soc. Rev.* **2012**, *41*, 3179−3192.

(12) Schatzschneider, U. Photoactivated Biological Activity of Transition-Metal Complexes. *Eur. J. Inorg. Chem.* **2010**, *2010*, 1451−1467.

(13) Butler, J. S.; Sadler, P. J. Targeted delivery of platinum-based anticancer complexes. *Curr. Opin. Chem. Biol.* **2013**, *17*, 175−188.

(14) Ko, J. K.; Auyeung, K. K. Identification of Functional Peptides from Natural and Synthetic Products on Their Anticancer Activities by Tumor Targeting. *Curr. Med. Chem.* **2014**, *21*, 2346−2356.

(15) Massaguer, A.; González-Cantó, A.; Escribano, E.; Barrabés, S.; Artigas, G.; Moreno, V.; Marchán, V. Integrin-targeted delivery into cancer cells of a Pt(IV) pro-drug through conjugation to RGD-containing peptides. *Dalton Trans.* **2015**, *44*, 202−212.

(16) Johnstone, T. C.; Wilson, J. J.; Lippard, S. J. Monofunctional and Higher-Valent Platinum Anticancer Agents. *Inorg. Chem.* **2013**, *52*, 12234−12249.

(17) Bruijnincx, P. C. A.; Sadler, P. J. Controlling platinum, ruthenium, and osmium reactivity for anticancer drug design. *Adv. Inorg. Chem.* **2009**, *61*, 1−62.

(18) Gasser, G.; Ott, I.; Metzler-Nolte, N. Organometallic Anticancer Compounds. *J. Med. Chem.* **2011**, *54*, 3−25.

(19) Smith, G. S.; Therrien, B. Targeted and multifunctional arene ruthenium chemotherapeutics. *Dalton Trans.* **2011**, *40*, 10793−10800.

(20) (a) Aliende, C.; Pérez-Manrique, M.; Jalón, F. A.; Manzano, B. R.; Rodríguez, A. M.; Cuevas, J. V.; Espino, G.; Martínez, M. A.; Massaguer, A.; González-Bártulos, M.; de Llorens, R.; Moreno, V. Preparation of new half sandwich ruthenium arene complexes with aminophosphines as potential chemotherapeutics. *J. Inorg. Biochem.* **2012**, *117*, 171−188. (b) Busto, N.; Valladolid, J.; Aliende, C.; Jalón, F. A.; Manzano, B. R.; Rodríguez, A. M.; Gaspar, J. F.; Martins, C.; Biver, T.; Espino, G.; Leal, J. M.; García, B. Preparation of Organometallic Ruthenium Arene Diaminotriazine Complexes as Binding Agents to DNA. *Chem. - Asian J.* **2012**, *7*, 788−801. (c) Valladolid, J.; Hortigüela, C.; Busto, N.; Espino, G.; Rodríguez, A. M.; Leal, J. M.; Jalón, F. A.; Manzano, B. R.; Carbayo, A.; García, B. Phenanthroline ligands are biologically more active than their corresponding ruthenium(II) arene complexes. *Dalton Trans.* **2014**, *43*, 2629−2645.

(21) Murray, B. S.; Babak, M. V.; Hartinger, Ch. G.; Dyson, P. J. The development of RAPTA compounds for the treatment of tumors. *Coord. Chem. Rev.* **2016**, *306*, 86−114.

(22) Kokan, Z.; Glasovac, Z.; Majerić Elenkov, M.; Gredičak, M.; Jerić, I.; Kirin, S. Y. Backdoor Induction of Chirality: Asymmetric Hydrogenation with Rhodium(I) Complexes of Triphenylphosphane-Substituted β-Turn Mimetics. *Organometallics* **2014**, *33*, 4005−4015.

(23) Stublla, A.; Potvin, P. G. Ruthenium(II) Complexes of Carboxylated Terpyridines and Dipyrazinylpyridines. *Eur. J. Inorg. Chem.* **2010**, *2010*, 3040−3050.

(24) Ashford, D. L.; Song, W.; Concepcion, J. J.; Glasson, Ch. R. K.; Brennaman, M. K.; Norris, M. R.; Fang, Z.; Templeton, J. L.; Meyer, T. J. Photoinduced Electron Transfer in a Chromophore−Catalyst Assembly Anchored to TiO_2. *J. Am. Chem. Soc.* **2012**, *134*, 19189−19198.

(25) McCafferty, D. G.; Bishop, B. M.; Wall, C. G.; Hughes, S. G.; Mecklenberg, S. L.; Meyer, T. J.; Erickson, B. W. Synthesis of redox

DOI: 10.1021/acs.inorgchem.7b01178
Inorg. Chem. 2017, 56, 13679−13696

derivatives of lysine and their use in solid-phase synthesis of a light-harvesting peptide. *Tetrahedron* **1995**, *51*, 1093−1106.
(26) Banerjee, T.; Rawalekar, S.; Das, A.; Ghosh, H. N. Interfacial Electron Transfer Dynamics of Two Newly Synthesized Catecholate Bound Ru(II) Polypyridyl-Based Sensitizers on TiO_2 Nanoparticle Surface − A Femtosecond Pump Probe Spectroscopic Study. *Eur. J. Inorg. Chem.* **2011**, *2011*, 4187−4197.
(27) Jarosz, P.; Du, P.; Schneider, J.; Lee, S. H.; McCamant, D.; Eisenberg, R. Platinum(II) Terpyridyl Acetylide Complexes on Platinized TiO_2: Toward the Photogeneration of H_2 in Aqueous Media. *Inorg. Chem.* **2009**, *48*, 9653−9663.
(28) Hu, X.; Smith, G. D.; Sykora, M.; Lee, S. J.; Grinstaff, M. W. Automated Solid-Phase Synthesis and Photophysical Properties of Oligodeoxynucleotides Labeled at 5′-Aminothymidine with Ru(bpy)$_2$(4-m-4′-cam-bpy)$^{2+}$. *Inorg. Chem.* **2000**, *39*, 2500−2504.
(29) Peek, B. M.; Ross, G. T.; Edwards, S. W.; Meyer, G. I.; Meyer, T. J.; Erickson, B. W. Synthesis of Redox Derivatives of Lysine and Related Peptides Containing Phenothiazine or Tris(2,2′-Bipyridine)ruthenium-(II). *Int. J. Pept. Protein Res.* **1991**, *38*, 114−123.
(30) Figgemeier, E.; Aranyos, V.; Constable, E. C.; Handel, R. W.; Housecroft, C. E.; Risinger, Ch.; Hagfeldt, A.; Mukhtar, E. Modification of electron transfer properties in photoelectrochemical solar cells by substituting {Ru(terpy)$_2$}$^{2+}$ dyes with thiophene. *Inorg. Chem. Commun.* **2004**, *7*, 117−121.
(31) Sáez, R.; Lorenzo, J.; Prieto, M. J.; Font-Bardia, M.; Calvet, T.; Omenaca, N.; Vilaseca, M.; Moreno, V. Influence of PPh_3 moiety in the anticancer activity of new organometallic ruthenium complexes. *J. Inorg. Biochem.* **2014**, *136*, 1−12.
(32) Yan, H.; Süss-Fink, G.; Neels, A.; Stoeckli-Evans, H. Mono-, di- and tetra-nuclear p-cymeneruthenium complexes containing oxalato ligands. *J. Chem. Soc., Dalton Trans.* **1997**, *22*, 4345−4350.
(33) Yi, X. Y.; Liu, B.; Jimenez-Aparicio, R.; Urbanos, F. A.; Gao, S.; Xu, W.; Chen, J. Sh.; Song, Y.; Zheng, L. M. Syntheses, Structures, and Magnetic Properties of Mixed-Valent Diruthenium (II,III) Diphosphonates with Discrete and One-Dimensional Structures. *Inorg. Chem.* **2005**, *44*, 4309−4314.
(34) Weil, M.; Bonneau, B. Crystal structures of $Na_2SeO_4{\cdot}1.5H_2O$ and $Na_2SeO_4{\cdot}10H_2O$. *Acta Crystallogr., Sect. E: Struct. Rep. Online* **2014**, *70*, 54−57.
(35) Milutinović, M. M.; Rilak, A.; Bratsos, I.; Klisurić, O.; Vraneš, D.; Gligorijević, N.; Radulović, S.; Bugarčić, Z. D. New 4′-(4-chlorophenyl)-2,2′:6′,2″-terpyridine ruthenium(II) complexes: Synthesis, characterization, interaction with DNA/BSA and cytotoxicity studies. *J. Inorg. Biochem.* **2017**, *169*, 1−12.
(36) Textor, M.; Oswald, H. R. Rontgenographirche und spektroskopische Untersuchungen an zwei Modifikationen von Dichloro-2,2′-dipyridyl- platin(II). *Z. Anorg. Allg. Chem.* **1974**, *407*, 244−256.
(37) Connick, W. B.; Henling, L. M.; Marsh, R. E.; Gray, H. B. Emission Spectroscopic Properties of the Red Form of Dichloro(2,2′-bipyridine)platinum(II). Role of Intermolecular Stacking Interactions. *Inorg. Chem.* **1996**, *35*, 6261−6265.
(38) Hazell, A.; Mukhopadhyay, A. Structure of bis(1,10-phenanthroline)platinum(II) dichloride trihydrate. *Acta Crystallogr., Sect. B: Struct. Crystallogr. Cryst. Chem.* **1980**, *36*, 1647−1649.
(39) Hannon, M. J. Supramolecular DNA recognition. *Chem. Soc. Rev.* **2007**, *36*, 280−295.
(40) Coury, J. E.; McFail-Isom, L.; Williams, L. D.; Bottomley, L. A. A novel assay for drug-DNA binding mode, affinity, and exclusion number: scanning force microscopy. *Proc. Natl. Acad. Sci. U. S. A.* **1996**, *93*, 12283−12286.
(41) Mier-Vinué, J.; Lorenzo, J.; Montaña, A. M.; Moreno, V.; Avilés, F. X. Synthesis, DNA interaction and cytotoxicity studies of cis-{[1, 2-bis(aminomethyl)cyclohexane]dihalo}platinum(II) complexes. *J. Inorg. Biochem.* **2008**, *102*, 973−987.
(42) Gao, F.; Chao, H.; Ji, L. N. DNA Binding, Photocleavage and Topoisomerase Inhibition of Functionalized Ruthenium(II)-Polypyridine Complexes. *Chem. Biodiversity* **2008**, *5*, 1962−1979.
(43) Groessl, M.; Tsybin, J. O.; Hartinger, Ch. G.; Keppler, B. K.; Dyson, P. J. Ruthenium versus platinum: interactions of anticancer metallodrugs with duplex oligonucleotides characterized by electrospray ionisation mass spectrometry. *JBIC, J. Biol. Inorg. Chem.* **2010**, *15*, 677−688.
(44) Miserachs, H. G.; Cipriani, M.; Grau, J.; Vilaseca, M.; Lorenzo, J.; Medeiros, A.; Comini, M. A.; Gambino, D.; Otero, L.; Moreno, V. Antitumor and antiparasitic activity of novel ruthenium compounds with polycyclic aromatic ligands. *J. Inorg. Biochem.* **2015**, *150*, 38−47.
(45) Ruiz, J.; Lorenzo, J.; Vicente, C.; Lopez, G.; Lopez-de-Luzuriaga, J. M.; Monge, M.; Avilés, F. X.; Bautista, D.; Moreno, V.; Laguna, A. New Palladium(II) and Platinum(II) Complexes with 9-Aminoacridine: Structures, Luminiscence, Theoretical Calculations, and Antitumor Activity. *Inorg. Chem.* **2008**, *47*, 6990−7001.
(46) Wu, P.; Wong, E. L.-M.; Ma, D.-L.; Tong, G. S.-M.; Ng, K.-M.; Che, C.-M. Cyclometalated Platinum(II) Complexes as Highly Sensitive Luminescent Switch-On Probes for Practical Application in Protein Staining and Cell Imaging. *Chem. - Eur. J.* **2009**, *15*, 3652−3656.
(47) (a) Utsuno, K.; Tsuboi, M.; Katsumata, S.; Iwamoto, T. Viewing of complex molecules of ethidium bromide and plasmid DNA in solution by atomic force microscopy. *Chem. Pharm. Bull.* **2001**, *49*, 413−417. (b) Pope, L. H.; Davies, M. C.; Laughton, C. A.; Roberts, C. J.; Tendler, S. J. B.; Williams, P. M. Atomic force microscopy studies of intercalation-induced changes in plasmid DNA tertiary structure. *J. Microsc.* **2000**, *199*, 68−78. (c) Riera, X.; Moreno, V.; Ciudad, C. J.; Noe, V.; Font-Bardía, M.; Solans, X. Complexes of Pd(II) and Pt(II) with 9-Aminoacridine: Reactions with DNA and Study of Their Antiproliferative Activity. *Bioinorg. Chem. Appl.* **2007**, *2007*, 98732−98746.
(48) Onoa, G. B.; Moreno, V. Study of the modifications caused by cisplatin, transplatin, and Pd(II) and Pt(II) mepirizole derivatives on pBR322 DNA by atomic force microscopy. *Int. J. Pharm.* **2002**, *245*, 55−65.
(49) Ruiz, J.; Cutillas, N.; Vicente, C.; Villa, M. D.; Lopez, G.; Lorenzo, J.; Aviles, F. X.; Moreno, V.; Bautista, D. New Palladium(II) and Platinum(II) Complexes with the Model Nucleobase 1-Methylcytosine: Antitumor Activity and Interactions with DNA. *Inorg. Chem.* **2005**, *44*, 7365−7376.
(50) Meyer-Almes, F. J.; Porschke, D. Mechanism of intercalation into the DNA double helix by ethidium. *Biochemistry* **1993**, *32*, 4246−4253.
(51) Selvakumar, B.; Rajendiran, V.; Uma, P.; Maheswari, H.; Stoeckli-Evans, M.; Palaniandavar, J. Structures, spectra, and DNA-binding properties of mixed ligand copper(II) complexes of iminodiacetic acid: The novel role of diimine co-ligands on DNA conformation and hydrolytic and oxidative double strand DNA cleavage. *J. Inorg. Biochem.* **2006**, *100*, 316−330.
(52) Lakowicz, J. R.; Webber, G. Quenching of fluorescence by oxygen. Probe for structural fluctuations in macromolecules. *Biochemistry* **1973**, *12*, 4161−4170.
(53) García-Giménez, J. L.; González-Álvarez, M.; Liu-González, M.; Macías, B.; Borrás, J.; Alzuet, G. Toward the development of metal-based synthetic nucleases: DNA binding and oxidative DNA cleavage of a mixed copper(II) complex with N-(9H-purin-6-yl)-benzenesulfonamide and 1,10-phenantroline. Antitumor activity in human Caco-2 cells and Jurkat T lymphocytes. Evaluation of p53 and Bcl-2 proteins in the apoptotic mechanism. *J. Inorg. Biochem.* **2009**, *103*, 923−934.
(54) Hernandez-Gil, J.; Ferrer, S.; Castiñeiras, A.; Lloret, F. A. Unique Discrete Tetranuclear Cu′−Cu(N-N)$_2$Cu−Cu′ Copper(II) Complex, Built from a μ^3 1,2,4-Triazolato-μ-carboxylato Ligand, as an Effective DNA Cleavage Agent. *Inorg. Chem.* **2012**, *51*, 9809−9819.
(55) Kellett, A.; O'Connor, M.; McCann, M.; McNamara, M.; Lynch, P.; Rosair, G.; McKee, V.; Creaven, B.; Walsh, M.; McClean, S.; Foltyn, A.; O'Shea, D.; Howea, O.; Devereux, M. Bis-phenanthroline copper(II) phthalate complexes are potent in vitro antitumour agents with 'self-activating' metallo-nuclease and DNA binding properties. *Dalton Trans.* **2011**, *40*, 1024−1027.
(56) Baguley, B. C.; LeBret, M. Quenching of DNA-ethidium fluorescence by amsacrine and other antitumor agents: a possible electron-transfer effect. *Biochemistry* **1984**, *23*, 937−943.
(57) Kelly, J. M.; Tossi, A. B.; McConnell, D. J.; OhUigin, C. A study of the interactions of some polypyridylruthenium(II) complexes with

DOI: 10.1021/acs.inorgchem.7b01178
Inorg. Chem. 2017, 56, 13679−13696

DNA using fluorescence spectroscopy, topoisomerisation and thermal denaturation. *Nucleic Acids Res.* **1985**, *13*, 6017−6034.
(58) Chen, L. M.; Liu, J.; Chen, J. C.; Shi, S.; Tan, C. P.; Zheng, K. C.; Ji, L. N. Experimental and theoretical studies on the DNA-binding and spectral properties of water-soluble complex $[Ru(MeIm)_4(dpq)]^{2+}$. *J. Mol. Struct.* **2008**, *881*, 156−166.
(59) Correia, I.; Roy, S.; Matos, C. P.; Borovic, S.; Butenko, N.; Cavaco, I.; Marques, F.; Lorenzo, J.; Rodríguez, A.; Moreno, V.; Pessoa, J. P. Vanadium(IV) and copper(II) complexes of salicylaldimines and aromatic heterocycles: Cytotoxicity, DNA binding and DNA cleavage properties. *J. Inorg. Biochem.* **2015**, *147*, 134−146.
(60) Chen, L. M.; Liu, J.; Chen, J. C.; Tan, C. P.; Shi, S.; Zheng, K. C.; Ji, L. N. Synthesis, characterization, DNA-binding and spectral properties of complexes $[Ru(L)_4(dppz)]^{2+}$ (L = Im and MeIm). *J. Inorg. Biochem.* **2008**, *102*, 330−341.
(61) Mardanya, S.; Karmakar, S.; Maity, D.; Baitalik, S. Ruthenium(II) and Osmium(II) Mixed Chelates Based on Pyrenyl−Pyridylimidazole and 2,2′-Bipyridine Ligands as Efficient DNA Intercalators and Anion Sensors. *Inorg. Chem.* **2015**, *54*, 513−526.
(62) Ramakrishnan, S.; Palaniandavar, M. Mixed-ligand copper(II) complexes of dipicolylamine and 1,10-phenanthrolines: the role of diimines in the interaction of the complexes with DNA. *J. Chem. Sci.* **2005**, *117*, 179−186.
(63) Mathur, S.; Tabassum, S. Template synthesis of novel carboxamide dinuclear copper (II) complex: spectral characterization and reactivity towards calf-thymus DNA. *BioMetals* **2008**, *21*, 299−310.
(64) Szacilowski, K.; Macyk, W.; Drzewiecka-Matuszek, A.; Brindell, M.; Stochel, G. Bioinorganic Photochemistry: Frontiers and Mechanisms. *Chem. Rev.* **2005**, *105*, 2647−2694.
(65) Juris, A.; Balzani, V.; Barigelletti, F.; Campagna, S.; Belser, P.; von Zelewsky, A. Ru(II) polypyridine complexes: photophysics, photochemistry, eletrochemistry, and chemiluminescence. *Coord. Chem. Rev.* **1988**, *84*, 85−277.
(66) Kaizu, Y.; Ohta, H.; Kobayashi, K.; Kobayashi, H.; Takuma, K.; Matsuo, T. Lifetimes of the lowest excited state of tris(2,2′-bipyridine)ruthenium(II) and its amphipathic derivative in micellar systems. *J. Photochem.* **1985**, *30*, 93−103.
(67) Garcia-Fresnadillo, D.; Georgiadou, Y.; Orellana, G.; Braun, A. M.; Oliveros, E. Singlet-Oxygen ($^1\Delta_g$) Production by Ruthenium(II) complexes containing polyazaheterocyclic ligands in methanol and in water. *Helv. Chim. Acta* **1996**, *79*, 1222−1238.
(68) Dobrucki, J. W. Interaction of oxygen-sensitive luminescent probes $Ru(phen)_3^{2+}$ and $Ru(bipy)_3^{2+}$ with animal and plant cells in vitro: Mechanism of phototoxicity and conditions for non-invasive oxygen measurements. *J. Photochem. Photobiol., B* **2001**, *65*, 136−144.
(69) Büchner, R.; Cunningham, C. T.; Field, J. S.; Haines, R. J.; McMillin, D. R.; Summertona, G. C. Luminescence properties of salts of the $[Pt(4'Ph\text{-}terpy)Cl]^+$ chromophore: crystal structure of the red form of $[Pt(4'Phterpy)Cl]BF_4$ (4′Ph-terpy 5 4′-phenyl-2,2′:6′,2″-terpyridine). *J. Chem. Soc., Dalton Trans.* **1999**, 711−718.
(70) Baraldi, P. G.; Bovero, A.; Fruttarolo, F.; Preti, D.; Tabrizi, M. A.; Pavani, M. G.; Romagnoli, R. DNA minor groove binders as potential antitumor and antimicrobial agents. *Med. Res. Rev.* **2004**, *24*, 475−528.
(71) Gilad, Y.; Senderowitz, H. Docking studies on DNA intercalators. *J. Chem. Inf. Model.* **2014**, *54*, 96−107.
(72) Al-Rashida, M.; Ahsen, S. In search of a docking protocol to distinguish between DNA intercalators and groove binders: genetic algorithm vs. shape-complementarity based docking methods. *RSC Adv.* **2015**, *5*, 72394−72404.
(73) Ricci, C. G.; Netz, P. A. Docking Studies on DNA-Ligand Interactions: Building and Application of a Protocol to Identify the Binding Mode. *J. Chem. Inf. Model.* **2009**, *49*, 1925−1935.
(74) Parveen, S.; Arjmand, F.; Ahmad, I. Enantiomeric in vitro DNA binding, pBR322 DNA cleavage and molecular docking studies of chiral L- and D-ternary copper(II) complexes of histidine and picolinic acid. *J. Photochem. Photobiol., B* **2014**, *130*, 170−178.
(75) Zhu, M.; Cui, X.; Zhang, S.; Liu, L.; Han, Z.; Gao, J. The structures, cytotoxicity, apoptosis and molecular docking controlled by the aliphatic chain of palladium(II) complexes. *J. Inorg. Biochem.* **2016**, *157*, 34−45.
(76) Icsel, C.; Yilmaz, V. T.; Kaya, Y.; Durmus, S.; Sarimahmut, M.; Buyukgungord, O.; Ulukaya, E. Cationic Pd(II)/Pt(II) 5,5-diethylbarbiturate complexes with bis(2-pyridylmethyl)amine and terpyridine: Synthesis, structures, DNA/BSA interactions, intracellular distribution, cytotoxic activity and induction of apoptosis. *J. Inorg. Biochem.* **2015**, *152*, 38−52.
(77) Alonso, H.; Bliznyuk, A. A.; Gready, J. E. Combining docking and molecular dynamic simulations in drug design. *Med. Res. Rev.* **2006**, *26*, 531−568.
(78) Fulmer, G. R.; Miller, A. J. M.; Sherden, N. H.; Gottlieb, H. E.; Nudelman, A.; Stoltz, B. M.; Bercaw, J. E.; Goldberg, K. I. NMR Chemical Shifts of Trace Impurities: Common Laboratory Solvents, Organics, and Gases in Deuterated Solvents Relevant to the Organometallic Chemist. *Organometallics* **2010**, *29*, 2176−2179.
(79) Bennett, M. A.; Huang, T.-N.; Matheson, T. W.; Smith, A. K.; Ittel, S.; Nickerson, W.; Fackler, J. F. Arene ruthenium(II) complexes formed by dehydrogenation of cyclohexadienes with ruthenium(III) trichloride. *J. Chem. Soc., Dalton Trans.* **1974**, 233−241.
(80) *SAINT v7.12a: Area-Detector Integration Program*; Bruker-Nonius AXS: Madison, WI, 2004.
(81) Sheldrick, G. M. *SADABS version 2004/1: A Program for Empirical Absorption Correction*; University of Göttingen: Göttingen, Germany, 2004.
(82) *SHELXTL-NT, version 6.12: Structure Determination Package*; Bruker-Nonius AXS: Madison, WI, 2001.
(83) Cohen, G.; Eisenberg, H. Viscosity and sedimentation study of sonicated DNA−proflavine complexes. *Biopolymers* **1969**, *8*, 45−55.
(84) Becke, A. D. Density-functional thermochemistry. I. The effect of the exchange-only gradient correction. *J. Chem. Phys.* **1992**, *96*, 2155−2160.
(85) Lee, C.; Yang, W.; Parr, R. G. Development of the Colle-Salvetti correlation-energy formula into a functional of the electron density. *Phys. Rev. B: Condens. Matter Mater. Phys.* **1988**, *37*, 785−789.
(86) Frisch, M. J.; et al. (see complete citation in the Supporting Information) *Gaussian 09*, rev. D.01; Gaussian, Inc.: Wallinford, CT, 2009.
(87) Andrae, D.; Häu*ß*ermann, U.; Dolg, M.; Stoll, H.; Preu*ß*, H. Energy-adjusted ab initio pseudopotentials for the second and third row transition elements. *Theor. Chim. Acta* **1990**, *77*, 123−141.
(88) Ehlers, A. W.; Böhme, M.; Dapprich, S.; Gobbi, A.; Höllwarth, A.; Jonas, V.; Köhler, K. F.; Stegmann, R.; Veldkamp, A.; Frenking, G. A set of f-polarization functions for pseudo-potential basis sets of the transition metals Sc-Cu, Y-Ag and La-Au. *Chem. Phys. Lett.* **1993**, *208*, 111−114.
(89) Schlegel, H. B. Optimization of equilibrium geometries and transition structures. *J. Comput. Chem.* **1982**, *3*, 214−281.
(90) Marenich, A. V.; Cramer, C. J.; Truhlar, D. G. Universal solvation model based on solute electron density and on a continuum model of the solvent defined by the bulk dielectric constant and atomic surface tensions. *J. Phys. Chem. B* **2009**, *113*, 6378−6396.
(91) Morris, G. M.; Huey, R.; Lindstrom, W.; Sanner, M. F.; Belew, R. K.; Goodsell, D. S.; Olson, A. J. AutoDock4 and AutoDockTools 4: Automated docking with selective receptor flexibility. *J. Comput. Chem.* **2009**, *30*, 2785−2791.
(92) Huey, R.; Morris, G. M.; Olson, A. J.; Goodsell, D. S. A semiempirical free energy force field with charge-based desolvation. *J. Comput. Chem.* **2007**, *28*, 1145−1152.
(93) Laskowski, R. A.; Swindells, M. B. LigPlot$^+$: multiple ligand-protein interaction diagrams for drug discovery. *J. Chem. Inf. Model.* **2011**, *51*, 2778−2786.
(94) Krieger, E.; Darden, T.; Nabuurs, S. B.; Finkelstein, A.; Vriend, G. Making optimal use of empirical energy functions: force-field parameterization in crystal space. *Proteins: Struct., Funct., Genet.* **2004**, *57*, 678−683.
(95) Krieger, E.; Koraimann, G.; Vriend, G. Increasing the precision of comparative models with YASARA NOVA—a self-parameterizing force field. *Proteins: Struct., Funct., Genet.* **2002**, *47*, 393−402.

DOI: 10.1021/acs.inorgchem.7b01178
Inorg. Chem. 2017, 56, 13679−13696